ELSEVIER

Clinical Biomechanics 16 (2001) 1–27

CLINICAL BIOMECHANICS

www.elsevier.com/locate/clinbiomech

Review paper

Biomechanics of the cervical spine Part 2. Cervical spine soft tissue responses and biomechanical modeling

Narayan Yoganandan [a,b,*], Srirangam Kumaresan [a,b], Frank A. Pintar [a,b]

[a] *Biomedical Engineering, Department of Neurosurgery, Medical College of Wisconsin, 9200 West Wisconsin Avenue, Milwaukee, WI 53226, USA*
[b] *Department of Veterans Affairs Medical Center, Milwaukee, WI, USA*

Received 7 February 2000; accepted 21 September 2000

Abstract

Objective. The responses and contributions of the soft tissue structures of the human neck are described with a focus on mathematical modeling. Spinal ligaments, intervertebral discs, zygapophysial joints, and uncovertebral joints of the cervical spine are included. Finite element modeling approaches have been emphasized. Representative data relevant to the development and execution of the model are discussed. A brief description is given on the functional mechanical role of the soft tissue components. Geometrical characteristics such as length and cross-sectional areas, and material properties such as force–displacement and stress–strain responses, are described for all components. Modeling approaches are discussed for each soft tissue structure. The final discussion emphasizes the normal and abnormal (e.g., degenerative joint disease, iatrogenic alteration, trauma) behaviors of the cervical spine with a focus on all these soft tissue responses. A brief description is provided on the modeling of the developmental biomechanics of the pediatric spine with a focus on soft tissues.

Relevance

Experimentally validated models based on accurate geometry, material property, boundary, and loading conditions are useful to delineate the clinical biomechanics of the spine. Both external and internal responses of the various spinal components, a data set not obtainable directly from experiments, can be determined using computational models. Since soft tissues control the complex structural response, an accurate simulation of their anatomic, functional, and biomechanical characteristics is necessary to understand the behavior of the cervical spine under normal and abnormal conditions such as facetectomy, discectomy, laminectomy, and fusion. © 2001 Published by Elsevier Science Ltd.

Keywords: Finite element modelling; Pediatric spine; Validation; Injury

1. Introduction

The osseous elements of the cervical vertebral column are connected by a variety of structures that collectively are known as the soft tissues of the cervical spine [1]. Ligaments of various types connect the vertebral bodies and the posterior elements of the cervical vertebrae, and span one or more segments, depending on the type of ligament and vertebral level. Fibrous capsules connect the articular processes of the synovial joints of the neck. At each segmental level, the anulus fibrosus of the intervertebral discs binds the adjacent vertebral bodies. Posteriorly, in the region of the uncinate processes, the connection is interrupted where the anulus is disrupted by transverse clefts that traditionally, but mistakenly, have been regarded as forming uncovertebral joints [2]. These soft tissues render the cervical spine compliant in that they allow for movement between the cervical vertebrae. However, they are also responsible for limiting the range of many movements under normal conditions. In the face of external (e.g., traumatic) loading, they are critical to maintaining the integrity of the cervical spine [1,3–7].

While sharing the general functions of enabling and limiting movement, the soft tissues of the cervical spine differ in structure and contribute differently to these functions. Ligaments consist of various amounts of collagen and elastin, arranged in essentially a uniaxial manner so as to resist tension. In contrast, the intervertebral discs consist of a proteoglycan nucleus designed to sustain compression loads, surrounded by a

* Corresponding author.
E-mail address: yoga@mcw.edu (N. Yoganandan).

0268-0033/01/$ - see front matter © 2001 Published by Elsevier Science Ltd.
PII: S0268-0033(00)00074-7

collagenous anulus fibrosus designed to resist tension, shear, and torsion [7–10].

The role of soft tissues in the biomechanics of the human cervical column can be assessed by investigating the external and internal responses of the spine. External responses can be defined as measurable parameters of the spinal structure (segment or column) under an externally applied load. For example, sagittal rotation under flexion-moment loading, i.e., moment-rotation curve is an external response. Similarly, compressive displacement under axial loading, i.e., force–deformation curve is an external response. These types of responses can be directly measured using experimental models such as a human cadaver spine segment [11–14] or spinal column [15,16]. In contrast, internal responses can be defined as the intrinsic parameter(s) of the spinal structure under externally applied load(s). For example, tensile stress in the intervertebral anulus fibers due to compressive loading is an internal response. Not only by definition but also because of the complex nature of spinal architecture, internal responses are not direct measurable quantities in an experiment.

Laboratory-driven experimental studies can delineate the external responses of the spine by studying isolated components (ligaments, etc.), segmented units (motion segments for disc evaluation, etc.) entire ligamentous cervical columns (evaluation of effects of spinal levels, injury, etc.), intact head–neck complexes (which includes passive musculature), and intact (whole body) human cadavers [13–27]. However, these studies are primarily limited in the sense that internal responses such as load sharing by the disc, and stresses and strains in the soft tissues cannot be determined. Mathematical analogues such as finite element models provide a unique opportunity to not only determine the external responses (verify/validate with experimental data), but they can also determine a number of internal responses (stresses, strains, strain energy density, etc.) [28–33]. Thus, finite element models serve as an adjunct to experimental models (external responses) and also complement experiments to determine internal responses. Furthermore, because of absolute repeatability and reproducibility, parametric studies are possible using finite element models.

Regardless of the type of response, internal or external, both the soft tissue and bony components contribute to spine biomechanical behavior. However, because of the significant differences in the mechanical properties of the soft tissues compared to the bony elements (hard tissues), the roles contributed by the various soft tissue structures (e.g., ligaments, discs, facet and uncovertebral joints) are different. Studies have clearly demonstrated that soft tissues govern the biomechanical responses of the cervical spine under external loading [34]. Therefore, it is important to delineate the characteristics and responses of the soft tissues of the spine.

With the above background, this review focuses on soft tissue structural responses with an emphasis on finite element mathematical models. The soft tissue structures included are the ligaments, intervertebral discs, zygapophysial joints, and uncovertebral joints. Specifically, each type of soft issue structure is discussed in terms of the following:

- its individual functional mechanical role,
- geometrical characteristics,
- material property, and
- modeling procedures.

Subsequent to these discussions, in a separate section, the effects of these individual soft tissue responses on the normal and abnormal (due to degenerative disorder, trauma, or iatrogenic alteration) behaviors of the cervical spine are discussed from a modeling perspective using representative finite element models. At the outset, it should be emphasized that significant differences exist in the anatomy and function, and mechanisms of load transfer and injury between the well-studied lumbar spine and relatively less-researched cervical spine. This is particularly true from a mathematical modeling perspective. Because of characteristic differences, a direct comparison/extrapolation from the low back to the neck should not be made.

2. Ligaments

2.1. Role

As stated earlier, ligaments are uniaxial structures that resist only tensile or distractive forces [7]. However, some ligaments are capable of resisting tensile forces in a range of directions because of their orientation. Since more than one type of ligament span adjacent vertebrae, their response is dependent on the nature of the external load vector. The anterior longitudinal ligament is most effective under an extension bending moment [35]. Interspinous ligaments are effective under a flexion moment. Depending on the severity, i.e., magnitude and application of the load vector, internal forces resisted by the various ligaments differ. Ligaments such as the posterior longitudinal ligament, which lie close to the center of rotation, respond with less force resistance than the anterior longitudinal ligament or the interspinous ligament. Ligaments are most effective when distracted along the direction of the fibers [35]. Thus, although ligaments are uniaxial mechanically, because of their complex anatomy, they respond under varying nature of external loads. Their internal response (strain or stress) secondary to loading is dependent on the mechanical properties of the particular ligament which, in turn, is a function of the constituents. Since elastin contributes to a more mechanical elastic behavior than collagen, lig-

aments with a higher proportion of elastin are more elastic (e.g., ligamentum flavum) [36,37].

2.2. Geometrical characteristics

In order to investigate the role of spinal ligaments and to model cervical spine behavior, it is important to quantify their geometry (origin and insertion/length and cross-sectional area) and material properties (stiffness, force–deflection, stress–strain). Radiographs can be used as an initial tool, although accuracy cannot be assured due to the integrated (e.g., one lateral view) and inferential nature of the imaging process. Computed tomography (CT) permits a higher level of geometrical measurement due to multiplanar (sagittal, axial) and multisectional (in a given plane) imaging flexibility. However, this method is also inferential with respect to soft tissue definitions [38]. Magnetic resonance imaging (MRI) is not routinely performed in a laboratory environment due to cost considerations. Furthermore, images with this technique for frozen human cadaver specimens is not a preferred methodology. Resolution of X-ray, CT, and MRI is also a factor for determining the geometry, i.e., length and cross-sectional areas of the ligaments.

Researchers have attempted to measure ligament geometry during gross dissection procedures [39]. However, significant difficulties are often encountered due to the presence of intervening tissues and body fluids. Other methods to obtain the geometry of anterior and posterior longitudinal ligaments of the mid-lower cervical spine have included the use of electromagnetic digitizer and laser micrometers [40], and micro dissection approach [41]. However, the efficacy of these systems has not been demonstrated to obtain data for upper cervical and internal ligaments. Cryomicrotomy techniques have been used to quantify ligament geometry [17,42]. Although this technique is destructive, it has been found to be superior because of its ability to obtain sequential images in a predetermined plane at very close intervals (of the order of a few microns, 1 mm = 1000 μm), thus describing the three-dimensional geometry. Cryomicrotomy techniques allow the specimen to be frozen in an undeformed, specific anatomic state (e.g., neutral alignment), thus preserving the in situ features of the spinal column. Because no dissection is done and the tissues can be frozen in their natural state, the anatomic integrity of the various hard and soft tissue structures and their relative position are not compromised [43]. Differences between the various structures are more clearly perceptible since extravasation does not occur immediately postmortem. Furthermore, the three-dimensional geometry of internal ligaments (ligamentum flavum) can be accurately obtained using this technique.

With regard to the definition of the specific ligament for measuring geometry (e.g., length), it is necessary to adopt an approach parallel to and consistent with the mathematical model. For example, the anterior and posterior longitudinal ligaments, because of their continuous nature in the human spinal column (traverse from upper cervical spine to sacrum), should be treated to span from mid-height of caudal vertebral body to mid-height of adjacent cephalad body at the specific vertebral level. This allows for a "continuous" ligament when longer column models are constructed. Researchers have identified this ligament to span the two neighboring endplates for determining length-related mechanical properties [40]. While this is acceptable from an experimental standpoint, use of this definition poses difficulties in a mathematical model as the portion of the ligament superior to the cephalad endplate and inferior to the caudal endplate cannot be simulated. Thus, caution is needed to define ligaments based on experiments which provide such information.

Ligament length and area definitions useful in mathematical modeling studies are as follows. As stated above, for length purposes, the longitudinal ligaments span the mid-height of adjacent vertebrae; ligamentum flavum and interspinous ligaments span the superior and inferior points of attachment of the two vertebrae; and joint capsules span from the superior tip of the caudal facet articulation to the inferior tip of the cephalad facet articulation [37]. For cross-sectional area purposes, maximum areas generally occur at mid-capsule height for joint capsules; locations midway between the adjacent spinous processes for interspinous ligaments; and mid-disc height for the two longitudinal ligaments [44]. Table 1 provides geometrical data, i.e., length and cross-sectional area of major cervical ligaments.

2.3. Material properties

From a mathematical modeling viewpoint, fundamental properties such as stiffness (structural property) or elastic modulus, a function of stress and strain (mechanical property), are generally required. These properties are obtained by subjecting the ligament under consideration to tensile loading. Experiments conducted with human cadaver cervical spine structures include isolated ligament tests and in situ bone–ligament–bone preparations [36,37,44,45]. Removal of the ligament from the spinal column for testing often results in damage to the structure and induces fixation failures [35]. In situ preparations have the unique advantage that the ligament under test is not isolated from its surroundings. In general, to perform these tests at a specific vertebral level, all soft tissues are transected carefully leaving the ligament under test to be the only structure to resist the externally applied uniaxial tension. Anatomical features are given importance during transection procedures. For example, the anterior longitudinal ligament is prepared by differentiating its fibers from the

Table 1
Length and cross-sectional area of cervical spine ligaments (Mean (SD)) [37][a]

	Area (mm^2)	Length (mm)
C2–C5		
ALL	11.1 (1.9)	18.8 (1.0)
PLL	11.3 (2.0)	19.0 (1.0)
LF	46.0 (5.8)	8.5 (0.9)
ISL	13.0 (3.3)	10.4 (0.8)
C5–T1		
ALL	12.1 (2.7)	18.3 (0.5)
PLL	14.7 (6.8)	17.9 (0.5)
LF	48.9 (7.9)	10.6 (0.6)
ISL	13.4 (1.0)	9.9 (0.7)

[a] ALL: anterior longitudinal ligament; PLL: posterior longitudinal ligament; LF: ligamentum flavum; ISL: interspinous ligament.

anulus of the disc, i.e., noting that the ligament fibers traverse in a superior–inferior direction while the disc anulus fibers are oblique. Vertebrae above and below the ligament under test are fixed, and a load cell (preferably six axis to insure uniaxial nature of force application) is placed at the distal end (Fig. 1). The specimen is subjected to axial tensile loading and the load-deformation response is obtained. A representative tensile force–deflection response is shown in Fig. 2 and discussed in detail in Appendix A [3–6,46]. Table 2 provides the failure force–deformation, energy, and stiffness for the various cervical spine ligaments in the upper cervical spine. The above-described tensile force–displacement response can be transformed into a stress–strain curve using the length and cross-sectional area geometrical parameters described in the earlier section. Table 3 includes data for middle and lower cervical spines, Fig. 3 illustrates the biomechanical responses, and Table 4 provides a bilinear modulus of elasticity data. In the interest of brevity, other data such as age, gender and loading rate are not included in all tabular data in this paper. The reader is referred to original articles for such information. The effects of age, gender and loading rate on cervical spine responses are reported by Pintar et al. [47].

The above-described force, deflection, energy, stiffness, stress, and strain parameters are applicable to (quasi) static tensile loading. In effect, these material property variables are applicable during day-to-day physiologic types of activities wherein the rate of load application is slow, i.e., sufficient time is allowed for the ligament structure to react (process of gradual reorientation of fibers during loading). However, as indicated in the introduction, the human body reacts and resists external loads in a dynamic environment (e.g., motor vehicle crashes, athletic activities) [27,47–58]. Ligament tears have been documented during high rates of loading; in contrast, avulsion of the ligament from the adjacent vertebra has been identified during slowly applied loads [36]. These studies indicate the rate-dependent or viscoelastic properties of the ligament structures. In particular, the failure force, stiffness, and energy have all been reported to increase with rate of loading (Fig. 4). For example, with increase in loading rate from 1.0 to 250 cm/s, the tensile failure load, stiffness, and energy for the anterior longitudinal ligament and ligamentum flavum of the cervical spine increased by a factor of 2–4. However, the failure distraction did not show such increasing tendencies with increasing loading rate. Similar trends have been reported in torque and rotation at the upper cervical joint with an increase in loading rate [59]. These results indicate that the spinal ligaments are deformation sensitive, i.e., once a stretch level is attained, regardless of the loading rate, failure is imminent. This property has also been observed in other soft tissue structures (e.g., liver, kidney, and thoracolumbar discs and ligaments) of the human body [60,61].

2.4. Modeling

The above-determined geometrical and mechanical properties of ligaments are being used in finite element models of the cervical spine [30,31,62]. Because of a lack of cervical ligament data, earlier researchers adopted data from lumbar spine [63] and lower extremity (foot–ankle) ligaments [64]. Varying assumptions have been used for simulating ligaments. Element idealizations have included spring or cable and membrane types. Table 5 includes a summary of some recent approaches used in modeling human cervical spine ligaments. Spring elements use a force–deflection curve [28] or stiffness as material property input [65,66], whereas membrane idealization uses a stress–strain curve [67] or modulus of elasticity [31,62,68] as the input. Depending on the complexity and need, finite element techniques allow the flexibility to choose linear, non-linear, and/or viscoelastic approaches.

If the analysis is limited to the linear domain, only a single number representing the linear stiffness or Young's modulus of elasticity is necessary and sufficient [30,32,69–71]. This approach has been shown to be efficacious at low-magnitude loading (e.g., 0.5 N m flexion–extension moment) to capture the spinal behavior. In contrast, at higher levels of pure moment and complex-eccentric loading, it is necessary to incorporate non-linear force–deflection/stress–strain responses in order to determine realistic spine behaviors [28,29]. Another important but frequently ignored issue is the effect of ligament pre-stress on the internal and external biomechanical responses of the spine. From functional and anatomical perspectives, ligaments have varying levels of pre-stress [45,72–74]. For example, the ligamentum flavum has more pre-stress than the anterior longitudinal ligament. Only recently have finite element studies begun to explore the effect of pre-stress [75].

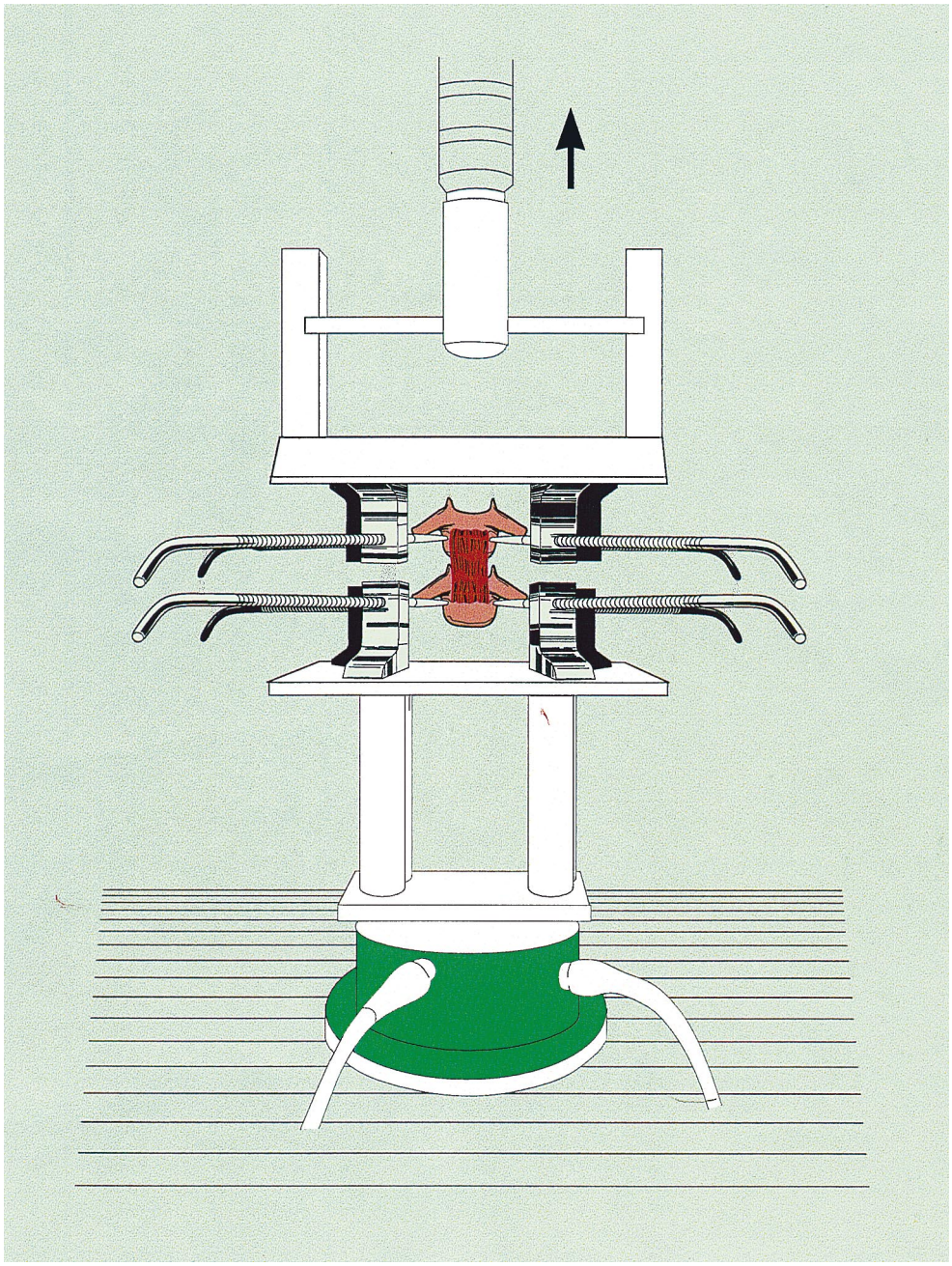

Fig. 1. Schematic of an in situ bone–anterior longitudinal ligament–bone preparation for tensile tests. A six-axis load cell is placed below the specimen to ensure the uniaxial nature of force application.

Both spring and truss element idealizations are capable of simulating the initial pre-stress in the ligament. Pre-stress increases the resting compression in the intervertebral disc and increases the overall structural stiffness [7]. Since ligaments are sensitive interconnecting structures, it is important to incorporate their complex (e.g., pre-stress, non-linear) characteristics to delineate accurate biomechanical responses of the cervical spine. The effects of the presence or absence of ligament structures on the external and internal responses of the other soft tissue structures (e.g., disc) are discussed in Section 6.

3. Intervertebral discs

3.1. Role

In contrast to ligaments which are uniaxial (tension), intervertebral discs respond to or experience multiple load vectors [7]. Under any external loading, with the exception of direct uniaxial tension (e.g., airbag loading), discs carry compressive forces in association with other components [1]. During normal physiologic conditions, the weight of the head places the C2–T1 discs in

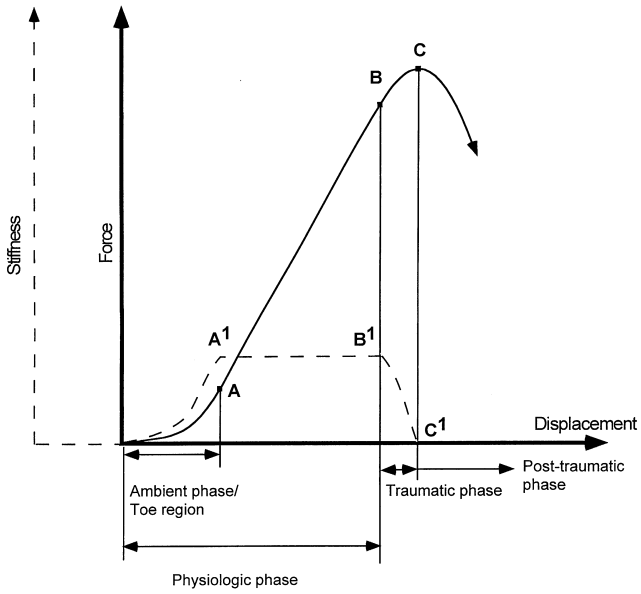

Fig. 2. Typical force–displacement (solid line) and stiffness displacement (dotted line) responses of a ligament. Non-linearity in the force–displacement behavior is apparent. OA denotes the ambient phase or toe region representing a highly non-linear curve corresponding to low stiffness; AB denotes the most linear phase (these two correspond to physiologic loading); BC denotes the traumatic phase (region of gradually decreasing stiffness); C denotes failure. Post-traumatic phase is represented by the portion of the curve beyond the traumatic phase (arrow). OA^1, A^1B^1, B^1C^1 denote the stiffness pattern in these phases. At the point of failure, the stiffness is zero. The physiologic, traumatic, and post-traumatic phases were renamed as neutral, elastic, and plastic zones, respectively [7].

some degree of compression. Thus, the fundamental functional mechanical role is to respond to compressive loading. Like ligaments, the internal response of the disc depends on the magnitude and nature of loading [28]. For example, under physiologic flexion loading, the anterior disc sustains compression while the load shared by the posterior anulus depends on severity of the flexion bending moment. Furthermore, because the head, which is approximately three times the weight of the neck, is eccentrically placed with respect to the cervical column, intervertebral discs do not carry/resist pure loading [20,76]. In other words, compression is associated with moment. The non-central anatomy of the nucleus pulposus also contributes to the dissimilar proportions of anterior and posterior anulus internal load sharing [8]. Thus, during physiologic and traumatic load applications, cervical intervertebral discs respond to a variety of load vectors including compression, bending, and tension [77].

3.2. Geometrical properties

As elucidated in the ligaments section, in order to investigate the role of the disc and to model spine behavior, geometrical characteristics have to be quantified. Radiographs, CT, and MRI provide reasonably accurate data on the geometrical characteristics of the disc, particularly the disc height [78]. Axial CT and MRI provide the cross-sectional areas of the disc. However, biomechanical investigators have quantified these geometrical data using human cadaver spines [79–82]. Table 6 includes a summary of the height of the cervical disc at its mid-depth, the ratio of anterior-to-posterior height, and cross-sectional areas of the nucleus pulposus and entire disc as a function of spinal level. As is true for ligament geometry, sequential anatomic cryomicrotomy sections provide three-dimensional geometrical data of disc nucleus and anulus. However, such in-depth quantification of disc geometry data has not been reported to the best of our knowledge. Studies are in progress in our laboratory to obtain these details [83].

3.3. Material properties

From a mathematical modeling viewpoint, force–displacement and properties such as stiffness and stress–strain (elastic modulus) are required. Unlike ligaments, material properties are needed in more than one mode because of the multi-modal behavior of the disc. Inter-

Table 2
Biomechanical data for ligaments in upper cervical spine (Mean (SD)) [83][a]

Spinal level	Type	Force (N)	Deformation (mm)	Energy (N m)	Stiffness (N/mm)
OC–C1	JC	320 (129)	9.9 (8.4)	2.03 (1.00)	32.6 (28.0)
OC–C1	AA–OM	232 (23)	18.9 (2.7)	2.44 (0.63)	16.9 (3.2)
OC-C1	PA–OM	83 (17)	18.1 (2.7)	0.87 (0.21)	5.7 (0.4)
C1–C2	ALL	263 (152)	11.8 (7.0)	2.07 (1.81)	24.0 (11.7)
C1–C2	JC	314 (143)	9.3 (4.5)	2.55 (2.55)	32.3 (23.5)
C1–C2	LF	111 (85)	9.6 (4.3)	0.58 (0.47)	11.6 (11.0)
OC–C2	TM	76 (44)	11.9 (2.5)	0.53 (0.31)	7.1 (2.3)
OC–C2	Apical	214 (115)	8.0 (5.3)	1.55 (1.53)	28.6 (29.0)
OC–C2	Alar	357 (220)	14.1 (7.2)	2.72 (1.77)	21.2 (15.7)
OC–C2	CLV	436 (69)	12.5 (4.9)	4.29 (2.98)	19.0 (0.2)

[a] JC = joint capsules; AA–OM = anterior atlanto–occipital membrane; PA–OM = posterior atlanto–occipital membrane; ALL = anterior longitudinal ligament; LF = ligamentum flavum; TM = tectorial membrane; CLV = cruciate ligament, vertical portion.

Table 3
Stress, strain, stiffness and energy properties of cervical spine ligaments (Mean (SD)) [37][a]

	Stress (MPa)	Strain (%)	Stiffness (N/mm)	Energy (N m)
C2–C5				
ALL	8.36 (1.76)	30.8 (5.0)	16.0 (2.7)	0.61 (0.25)
PLL	6.29 (2.28)	18.2 (3.2)	25.4 (7.2)	0.21 (0.10)
LF	2.64 (0.79)	77.0 (12.9)	25.0 (7.0)	0.49 (0.17)
ISL	2.97 (0.76)	60.9 (11.2)	7.74 (1.6)	0.13 (0.03)
C5–T1				
ALL	12.0 (1.41)	35.4 (5.9)	17.9 (3.4)	0.54 (0.13)
PLL	12.8 (3.38)	34.1 (8.8)	23.0 (2.4)	0.40 (0.11)
LF	2.64 (0.34)	88.4 (13.1)	21.6 (3.7)	0.91 (0.22)
ISL	2.88 (0.74)	68.1 (13.8)	6.4 (0.7)	0.18 (0.06)

[a] ALL: anterior longitudinal ligament; PLL: posterior longitudinal ligament; LF: ligamentum flavum; ISL: interspinous ligament.

vertebral disc responses are obtained by subjecting a functional spinal unit (vertebra–disc–vertebra) [84] or a disc segment (body–disc–body) [13,85] to external loading. Because of the importance of compressive loading, studies have initially focused on the gross response of the disc under this mode. Typically, the specimens are fixed at the inferior end and compression (or tension) loading is applied to the superior end using a materials testing machine (e.g., electrohydraulic testing device) until failure (Fig. 5). Failure is identified as the point on the load–deflection curve at which an increase in compressive displacement (or distraction) results in a decrease of the resistive force. The force–displacement response is non-linear, typical of biological materials, and similar to the behavior shown in Fig. 2. Using the same principles, it is possible to transform the force–displacement response into a stiffness–deflection response and delineate disc biomechanics. As before, the onset of a reducing stiffness following the attainment of the peak force in the physiologic loading response (point

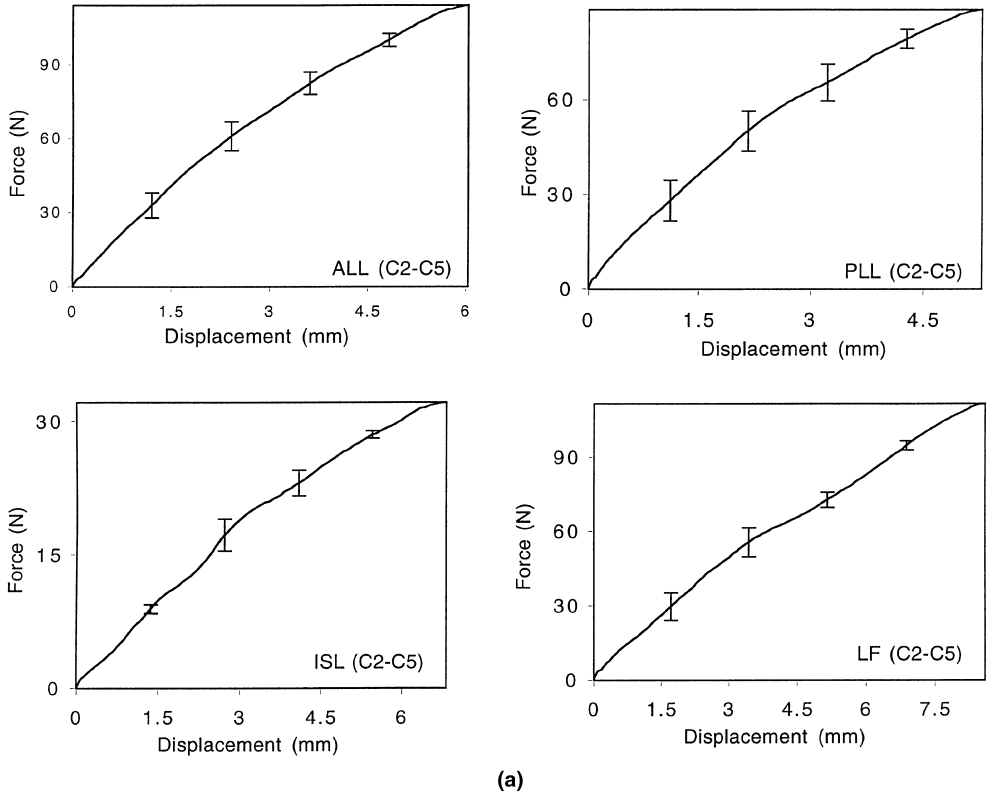

Fig. 3. (a) Tensile force–deflection properties of cervical spine ligaments (C2–C5). (b) Tensile force–deflection properties of cervical spine ligaments (C5–T1).

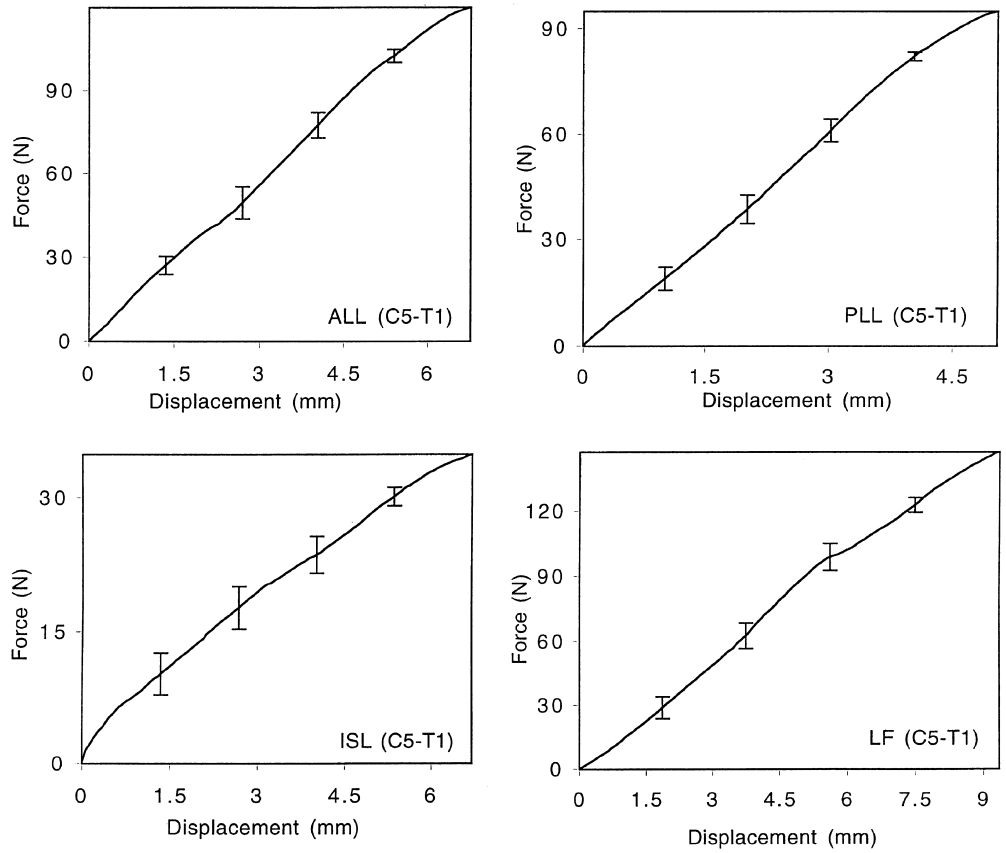

Fig. 3. (Continued).

C/C[1] in Fig. 2), i.e., at the beginning of the traumatic loading phase, indicates injury to the disc segment [3,4]. This microlevel trauma, not apparent on radiographs, occurs to the endplate component of the disc. It should be noted that disc material seldom fails under compression, but the endplate ruptures [46,52]. Using these force–deflection responses, parameters such as microfailure load, stiffness in the most linear, physiologic range, and energy absorption characteristics have been determined under compression. Table 7 includes biomechanical data under compression and tension.

As described later, it is important to determine the material properties of the individual constituents of the disc (e.g., anular fibers) in addition to the above-deter-

Table 4
Young's modulus (MPa) of elasticity of cervical spine ligaments [37][a]

Type	E_1	E_2	ε_{12}
C2–C5			
ALL	43.8	26.3	12.9
PLL	40.9	22.2	11.1
LF	3.1	2.1	40.7
ISL	4.9	3.1	26.1
C5–T1			
ALL	28.2	28.4	14.8
PLL	23.0	24.6	11.2
LF	3.5	3.4	35.3
ISL	5.0	3.3	27.0

[a] ε_{12} denotes the strain transition between the two bilinear moduli (E_1 and E_2).

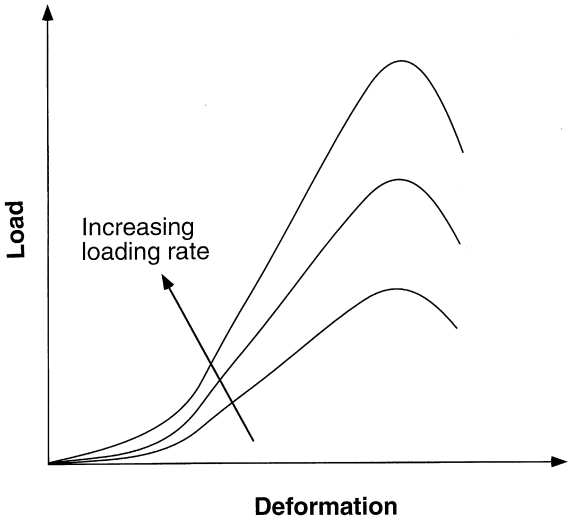

Fig. 4. Rate-dependent mechanical response of soft tissue structures such as ligaments. Note the shift of the curve toward the ordinate indicating the stiffening response with increasing load/strain rate.

Table 5
Inclusion of spinal ligaments in mathematical models[a]

Author	Year	Ligaments	Element idealization	Material properties	Reference
Williams and Belytschko	1983	ALL, PLL, LF	Non-linear spring	$T = K_1 e^{K2d}$ T – ligament force; d – elongation; K_1, K_2 – constants	[91]
Saito et al.	1991	ALL, PLL, ISL, SSL, LF	Linear triangle (two-dimensional)	Same properties for all ligaments: E: 185 MPa (tension), l (compression), γ 0.36 (tension), 0.45 (compression)	[68]
Kleinberger	1993	ALL, PLL, LF, ISL, SSL	Linear spring	k (N/mm) ALL – 33.0, PLL – 20.4, ISL – 25.3, SSL – 23.7, LF – 27.2 For all ligaments: γ 0.49	[65]
Dauvilliers et al.	1994	ALL, PLL, LF, ISL, SSL	Linear spring-damper	For all ligaments: k 50 N/m	[66]
Yoganandan et al.	1995–1997	ALL, PLL, CL, ISL, LF	Linear and axial	E (MPa) ALL: 11.9–54.5, PLL: 12.5–30, ISL: 1.5–3.4, CL: 2–7.7, LF: 1.5–2.4 For all ligaments: γ 0.39	[30,69–71]
Nitsche et al.	1996	ALL, PLL, LF, SSL, ITL, TL	Linear membrane	Same properties for all ligaments: (E: 2*52 MPa, γ 0.22)	[64]
de Jager et al.	1997	ALL, PLL, CL, LF, ISL	Non-linear straight line	$F_l = [F_{el}(\varepsilon) + b_l \, d\varepsilon/dt$ for $\varepsilon > 0]$, [0 for $\varepsilon < 0$] F_l – ligament force b_l – damping coefficient (300 N s/m) ε – strain F_{el} – non-linear force–strain curve	[63]
Maurel et al.	1997	ALL, PLL, CL, LF, ISL, SSL	Linear cable	E (MPa) ALL – 10, PLL – 20, CL – 20, LF – 50, ISL – 3, SSL – 3	[31]
Yang et al.	1998	ALL, PLL, AL, SSL, LF, CL, ISL, TL	Membrane and bar	E (MPa) ALL – 11.4, PLL – 9.12, SSL – 8.55, ISL – 4.56, LF – 5.7, AL – 11.4, TL – 17.1, CL – 22.8 For all ligaments: γ 0.4	[67]
Goel et al.	1998	ALL, PLL, ISL, CL, LF	Bilinear cable	E (MPa) ALL 15 (<12%) 30 (>12%), PLL 10 (<12%) 20 (>12%), ISL 4 20–40%) 8 (>40), CL 7 (<30%) 30 (>12%), LF 5 (<25%) 10 (>25%) For all ligaments: γ 0.3	[88]
Kumaresan et al.	2000	ALL, PLL	Spring, truss	Ligament initial pre-stress spring – k 7.5 N/mm truss – E 4.31 MPa	[75]
Kumaresan et al.	1997–2000	ALL, PLL, LF, ISL, CL	Non-linear cable	Data from in-house laboratory tests (see Figs. 3 and 7 in text)	[28,29,130, 131,133]

[a] ALL: anterior longitudinal ligament; PLL: posterior longitudinal ligament; LF: ligamentum flavum; ISL: interspinous ligament; CL: capsular ligament; SSL: supraspinous ligament; TL: transversal ligament; ITL: intertransversal ligament; AL: alar ligament; γ: Poisson's ratio; E: modulus of elasticity; k: stiffness.

mined gross responses under compression and tension. For this purpose, from a mathematical modeling viewpoint, it is necessary to establish the force–displacement/stress–strain response of the anular fibers in tension and ground matrix in compression [86,87]. Since data from cervical spine discs are not currently available, similar information from lumbar disc is used in current finite element models [29,88]. A uniaxial tension test is typically conducted on a predetermined sample of a specific length and thickness from a specific region of the disc at

Table 6
Geometrical properties of intervertebral disc [79,83]

Level	Disc area (mm^2)	Nucleus area (mm^2)	Average disc height (mm)	Ratio of posterior height to anterior height
C2–3	108–262	54–134	3.8–5.8	0.53–0.61
C3–4	98–442	55–119	4.5–6.0	0.47–0.55
C4–5	118–332	33	4.6–6.5	0.43–0.51
C5–6	129–440	68–148	4.2–7.2	0.41–0.49
C6–7	168–502	139–251	5.0–7.5	0.61–0.69
C7–T1	188–482	121–233	4.5–7.2	0.59–0.67

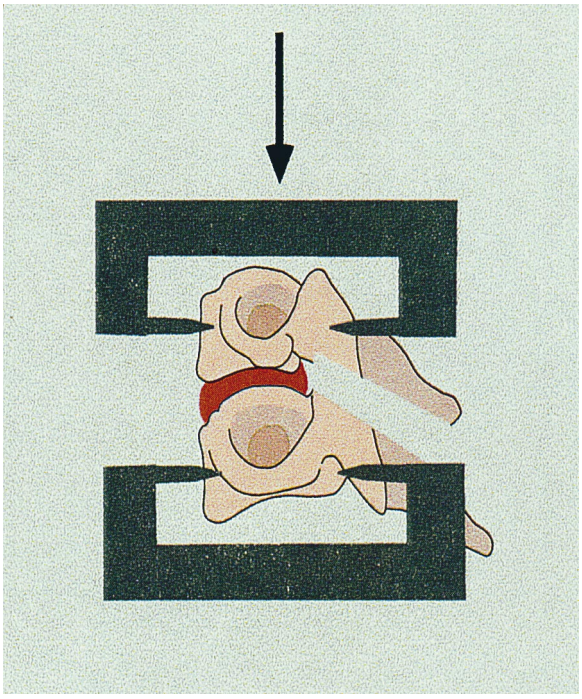

Fig. 5. Disc-segment used to determine gross force–deflection properties of the intervertebral unit in axial compression.

a quasi-static loading rate [86]. Using an a priori gauge length, force–deflection characteristics are converted to stress–strain responses. The properties of the ground substance are obtained using the initial part (ambient phase/toe region, Fig. 2) of the stress–strain response of the disc in compression [87]. Young's modulus of elasticity for the anulus ground substance ranged from 3.4 to 4.7 MPa [29,88–90]. However, for the anulus fibers, a linear Young's modulus of 450 to 500 MPa is routinely chosen.

3.4. Modeling

As in the case of ligaments, several modeling approaches have been used to simulate the disc. For example, a composite, single-entity definition that incorporates Young's modulus of elasticity in compression and tension has been used [64–66,91]. This definition does not differentiate between the properties of the nucleus, anulus ground substance, and fibers. Solid finite elements have been selected for this purpose. More complex and realistic models have attempted to simulate the three structural constituents of the disc. The nucleus is routinely modeled using incompressible fluid elements [28,32]. Solid elements with a Poisson's ratio close to 0.5 have also been used to represent the nucleus [88]. With regard to the anulus component, fibers have been simulated using reinforced bar (rebar) or cable elements and ground substance with solid elements (Table 8). It is possible, with this differentiation, to determine internal biomechanical parameters such as fiber strain and stresses, load sharing in the different regions of the disc, and stresses in the ground substance, and correlate these with clinically related topics such as formation of osteophytes, disc herniation, and effects of discectomy. These are discussed in Section 6.

4. Zygapophysial joint

4.1. Role

Like the intervertebral disc, zygapophysial joints respond to multiple load vectors [53]. Together with the disc, zygapophysial joints resist compressive forces in the subaxial cervical spine [89]. The share of the compressive load resisted by the two zygapophysial joints at any cervical level depends on the orientation of the joint and eccentricity of the external compressive force [92]. From this point of view, zygapophysial joints provide a complementary role to the disc [93]. The load shared by the joint changes with the degeneration of the joint, disc, and vertebral body [78]. Because of the oblique orientation of the facet processes, the external load is resisted by normal and shear forces in the joint [94]. Thus, antero–posterior shear loading is supported. Because the zygapophysial joints are replete with pain-sensitive structures, any deviation from its normal physiologic function due to degenerative disorders [95] or trauma [1,96–102] may lead to facet-induced pain in the head,

Table 7
Failure data of intervertebral disc under tension test [15]; biomechanical data of intervertebral disc under compression test [83]

Level	Force (N)	Deformation (mm)	Energy (J)	Stiffness (N/mm)
A – Under tension test				
C2–C3	636	11.4	3.70	63.5
C3–C4	636	12.1	4.41	69.8
C4–C5	571	9.3	5.50	66.8
C5–C6	391	12.7	2.64	22.0
C6–C7	505	10.0	3.32	69.0
C7–T1	535	11.3	3.28	82.2
B – Under compression test				
C2–C3	602	1.4	0.31	637.5
C3–C4	683	1.5	0.33	765.3
C4–C5	777	1.6	0.40	784.6
C5–C6	664	1.6	0.33	800.2
C6–C7	673	1.7	0.34	829.7
C7–T1	910	1.6	0.48	973.6

neck, and shoulders depending on the level at which integrity of the joint is compromised [18,103,104]. Furthermore, due to posterior placement in the vertebra, it is a major stabilizing structure for other tissues in the region of the neck. Zygapophysial joints also act to limit the torsion of the disc, although this is more predominant in the thoracolumbar spine [105]. The capsular ligament is an important local stabilizer of the zygapophysial joint [11,106–108]. The role of ligaments was discussed earlier. The coupling motion of the lower cervical spine in lateral bending and axial rotation is determined by the oblique orientation of the zygapophysial joint, together with the uncovertebral joints (discussed later).

4.2. Geometrical characteristics

Geometrical properties, such as the length and cross-sectional area, can be obtained from imaging techniques such as X-rays, CT, and MRI. Vertebral gross-dissection evaluations have determined the bony areas of the superior and inferior processes at each level [109,110]. However, as indicated earlier, cryomicrotomy and gross-dissection procedures have been used with added success [44]. A distinct advantage of cryomicrotomy is that tissues not easily quantified by other procedures such as CT, MRI, and even gross-dissection can be evaluated with greater detail and accuracy. The thickness and profile of the articular cartilage can be determined using this sequential anatomic sectioning technique. Table 9 provides the geometrical data of the zygapophysial joint as a function of spinal level. For modeling purposes, the gap between the opposing cartilage is filled with synovial fluid [111]. The geometry of the capsular ligaments that surround the facet capsule is obtained from cryomicrotomy [37]. A schematic of the zygapophysial joint components (exploded view) is illustrated (Fig. 6).

4.3. Material property

Since zygapophysial joints consist of synovial fluid, synovial membrane, articular cartilage adjacent to the bony facet of the articular pillar and a fibrous capsule (Fig. 6) [112], as well as intra-articular meniscoids [113], the material properties of these individual components must be defined, in order to simulate them in a finite element model. Because the zygapophysial joint composition is similar to other joints, and since material properties of this cervical structure have not been determined experimentally, data have been used from other similar components of the human body [114]. Using stress–strain curves, linear Young's modulus of elasticity values has been determined to define the articular cartilage and synovial membrane [111]. Fluid density has been used to define the synovial fluid. In contrast, for the ligaments that surround the zygapophysial joint, mechanical properties have been determined (Table 10, Fig. 7). Table 10 provides a summary of biomechanical data of zygapophysial joint capsules.

4.4. Modeling

A majority of finite element simulations of the zygapophysial joint include facet bone, capsular ligament, and air gap between the two cartilages (Table 11) [31,63,88]. Facet bone is modeled as a solid element and included in the vertebra simulation. Capsular ligament is modeled as described in the section on ligaments. The space between the two cartilage is defined using sliding or contact gap elements. Definitions of the articular cartilage are lacking in these models [31,63,88]. More recently, however, advanced modeling approaches have incorporated the simulation of articular cartilage using solid elements, synovial fluid using fluid elements, and synovial membrane using membrane elements [111]. It

Table 8
Inclusion of intervertebral discs in mathematical models[a]

Author	Year	Disc component	Element idealization	Material properties	Reference
Williams and Belytschko	1983	Composite single (anulus, nucleus)	Beam	k – 3.5E + 5 – 20E + 5 N/m, 9–84 N m/rad	[91]
Saito et al.	1991	Anulus	2-D triangle	E – 40.0, γ 0.49	[68]
		Nucleus	2-D triangle	E – 200.0, γ 0.49	
Kleinberger	1993	Composite anulus, nucleus and fiber	solid	E – 3.4, γ 0.49	[65]
Dauvilliers et al.	1994	Composite anulus and nucleus	Solid	E – 200.0, γ 0.29	[66]
		Anulus fiber	Spring-damper (tension)	k – 50–75 N/m	
Yoganandan et al.	1995–1997	Anulus ground substance	Solid	E – 3.4, γ 0.4	[30,69–71]
		Nucleus pulposus	Solid	E – 3.4, γ 0.49	
Nitsche et al.	1996	Composite anulus, nucleus	Solid	E – 100.0, γ 0.4	[64]
de Jager et al.	1997	Composite single anulus, nucleus	Linear viscoelastic elements	k – 68–492 N/mm, γ 0.45	[63]
				k – 0.21–0.42 N m/deg. γ 0.3	
				c – 1000 N s/m, 1.5 N ms/rad	
Maurel et al.	1997	Composite anulus	Solid	E – 2.5 MPa, γ 0.45	[31]
		Anulus fiber (lateral)	Cable (tension)	E – 10.0 MPa	
		Anulus fiber (anterior and posterior)	Cable (tension)	E – 110.0 MPa	
Yang et al.	1998	Anulus	Solid	E – 98.0 MPa, γ 0.45	
		Nucleus	Solid	G_1 – 2 MPa	[67]
				G_2 – 1.4 MPa	
				K – 2200	
Goel et al.	1998	Anulus ground substance	Solid	E – 4.2 MPa, γ 0.45	[88]
		Anulus fiber	Rebar (tension)	E – 450.0 MPa, γ 0.30	
		Nucleus pulposus	Solid	E – 1.0 MPa, γ 0.499	[28,29,130, 131,133]
Kumaresan et al.	1997–2000	Anulus ground substance	Solid	E – 4.7, γ 0.45	
		Anulus fiber	Rebar (tension)	E – 500.0	
		Nucleus pulposus	fluid	K – 1666.7	

[a] k: Stiffness; K: bulk modulus; G_1: short-term shear modulus; G_2: long-term shear modulus; c: damping coefficient.

has been shown that inclusion of the fluid element provides more realistic internal response (e.g., stress) characteristics than other procedures. With these individual component simulations, the role of the zygapophysial joint in the normal and abnormal (e.g., iatrogenic alterations, disease, trauma) biomechanics of the cervical spine can be studied using external and internal response variables. These are discussed in Section 6.

5. Uncovertebral clefts

5.1. Role

Located in the vertebral body–disc–vertebral body medium, from C2 to T1, are clefts (formerly referred to as Luschka's joints) (Fig. 8) [2,115]. The clefts are not formed at birth, and therefore, do not constitute joints. They arise late in childhood; become more evident in the young adult; and increase in size with advancing age, extending to meet in the midline to produce a transverse fissure across the back of the disc. They arise in the anulus fibrosus between the uncinate process of the lower vertebral body laterally and the saddle contour of the caudolateral aspect of the upper vertebral body medially. The clefts allow for a large degree of movement between the vertebral bodies and through the intervertebral disc [116–118], particularly in axial rotation [119]. The clefts enable the disc to accommodate the coupling of lateral bending and axial rotation that is governed by the zygapophysial joints [120].

Table 9
Geometrical properties of zygapophysial joint [109,110][a]

		Anteroposterior diameter (mm)	Lateral diameter (mm)
C1	Superior	17–31	9–16
	Inferior	14–22	12–18
C2	Superior	4–23	12–23
	Inferior	8–18	7–17
C3	Superior	5–20	7–16
	Inferior	4–20	6–16
C4	Superior	4–21	4–16
	Inferior	5–18	7–17
C5	Superior	6–18	6–17
	Inferior	7–16	7–17
C6	Superior	6–16	8–18
	Inferior	7–17	7–19
C7	Superior	7–18	6–19
	Inferior	6–20	8–22

[a] Note: Dimension assumes zygapophysial joint surface as an ellipse.

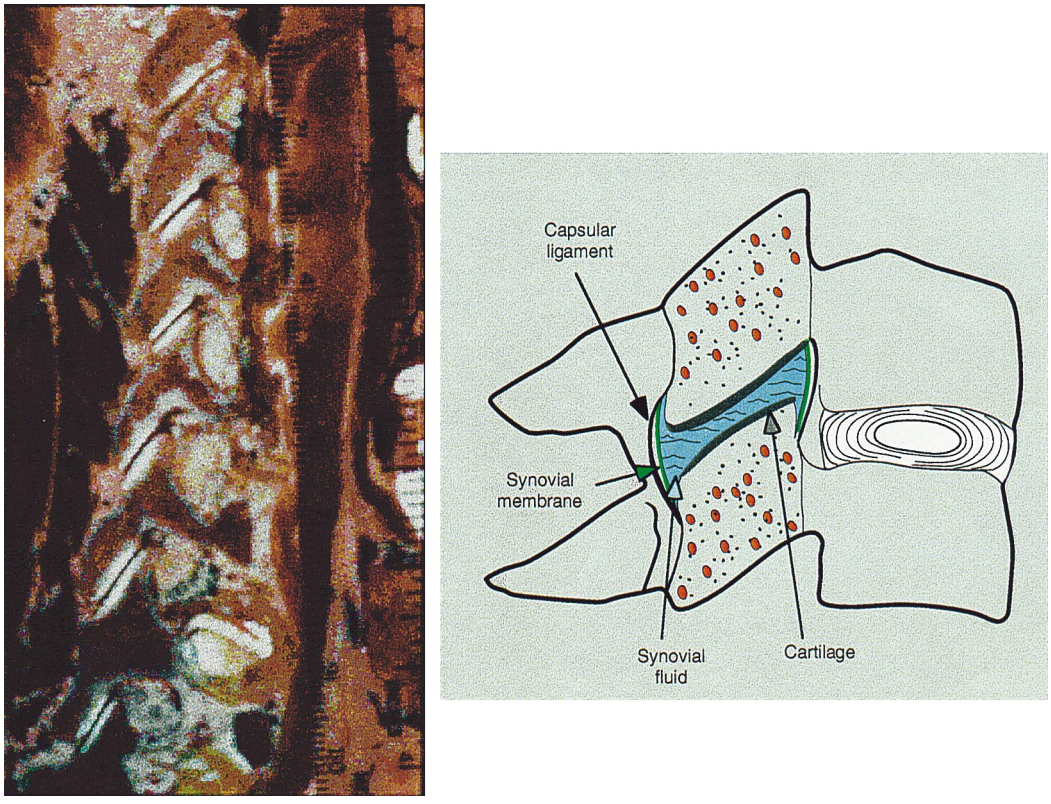

Fig. 6. Left: sagittal frozen anatomic section of the human cervical spine showing the zygapophysial joint. Right: illustration of zygapophysial joint in magnified view. The components of the zygapophysial joint such as the articular cartilage, synovial fluid and synovial membrane were included in the finite element model based on the details obtained from these anatomic sections.

5.2. Geometrical characteristics

Although the location of the clefts can be inferred from radiographs, CT, and MRI, it is difficult to quantify their three-dimensional geometrical characteristics from these media. For the purposes of modeling, directly obtained anatomical data are required. As an initial step, two-dimensional geometrical details were obtained from radiographs [118]. Subsequently, three-dimensional characteristics were determined in a cadaver using cryomicrotomy (Fig. 9) [2]. The data are the anteroposterior length, medial–lateral depth, and superior–inferior height of each cleft, from C2 to T1 (Table 12).

Table 10
Biomechanical data of joint capsules (Mean (SD)) [37]

	Stress (MPa)	Strain (%)	Stiffness (N/mm)	Energy (N m)
C2–C5	5.67 (1.47)	148.0 (28.5)	33.6 (5.5)	1.49 (0.54)
C5–T1	7.36 (1.27)	116.0 (19.6)	36.9 (6.1)	1.50 (0.37)

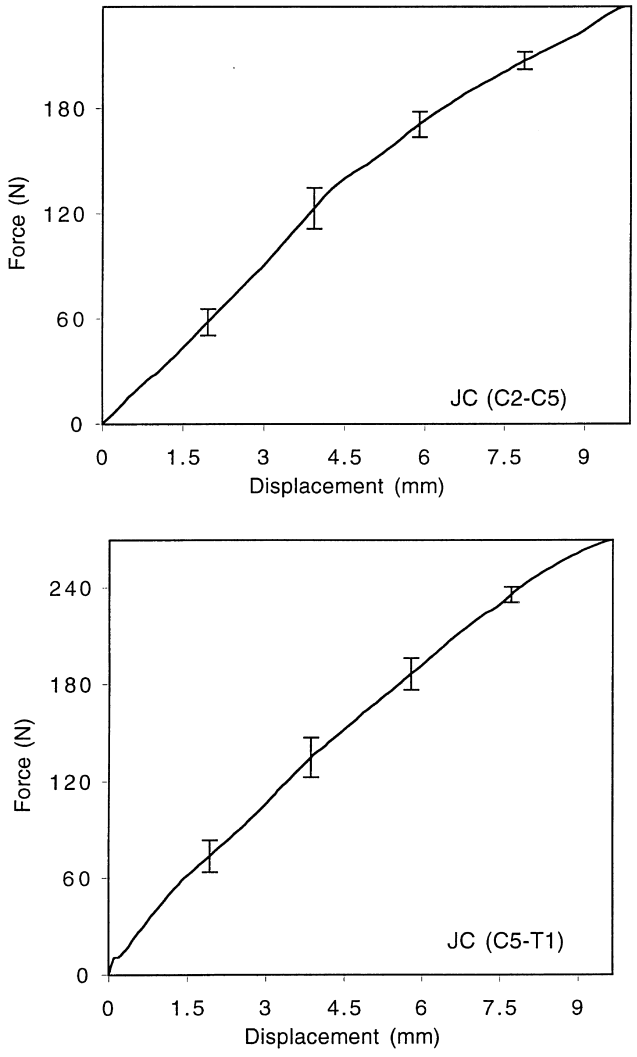

Fig. 7. Force–deflection responses of joint capsules (Top: C2–C5; Bottom: C5–T1).

5.3. Material properties and modeling

To the best of our knowledge, specific experiments have not been conducted to determine the individual mechanical properties of these clefts. However, in the belief that they are similar to the zygapophysial joints, investigators have used approaches analogues to those used for the zygapophysial joints [28]. In simulating clefts, gap elements have been used [62]. More sophisticated fluid element representations are also adopted (Table 13).

6. Effects of soft tissue responses on spine behavior: normal and abnormal

Finite element analysis offers a unique modeling approach to understand the role of the soft tissues in normal and abnormal conditions of the spine [32,70,89,90,121]. Because of the varying biomechanical properties (e.g., synovial fluid, cartilage) and complex, irregular, anatomic structural features, other models such as lumped parameter and continuum models are limited in their applications [32]. It is a relatively easy task to determine the contribution of one soft tissue component or a portion of a soft tissue component (e.g., full versus partial discectomy) on the internal and external biomechanical responses once the initial model is developed and validated. A brief summary of some of the recent finite element models is given below with regard to the delineation of the biomechanical response. As is applicable to earlier discussions, the intent is to demonstrate the role of soft tissue responses using modeling approaches.

6.1. Role of zygapophysial joints: graded unilateral and bilateral facetectomies

An anatomically accurate, fully three-dimensional, 10 966-noded finite element model of a C4–C5–C6 spinal unit (Fig. 10) was constructed by our group [30,107]. It was validated under pure moment loading of 1.8 N m in physiologic flexion, extension, lateral bending, and axial torsion modes. Bony data for the model were obtained from close-up 1.0-mm axial, coronal, and sagittal CT scans; soft tissue characteristics were incorporated using close-up sequential cryomicrotomy images extracted from a 33-year-old human cadaver. The effects of intact (normal), and 25%, 50%, 75%, and 100% single-level unilateral and bilateral facetectomies on the external moment-rotation and internal anulus stress in the two adjacent discs were studied. The effects of unilateral facetectomy (all grades) were less than those of bilateral facetectomy. Cervical rotations increased with increasing degree of zygapophysial joint resections. The greatest change occurred between 50% and 75% resection (Fig. 11(a)). These external responses were compared with the literature [11,106,122,123]. With regard to the internal disc stress, although a sim-

Table 11
Inclusion of zygapophysial joint in mathematical models[a]

Author	Year	Zygapophysial joint components	Element idealization	Material properties	Reference
Williams and Belytschko	1983	Gap between facet bones	Pentahedral	Compression k 10E + 5 N/m Tension k 0.5E + 5 N/m	[91]
Saito et al.	1991	Gap between facet bone	2-D triangle	E 30 MPa, γ 0.45	[68]
Kleinberger	1993	Gap between facet bones	Solid	E 3.4 MPa, γ 0.49	[65]
Dauvilliers et al.	1994	Gap between facet bones	Spring-damper	k 50 N/m	[66]
Yoganandan et al.	1995–1997	Articular cartilage	Solid	E 3.4 MPa, γ 0.4	[30,69–71]
Nitsche et al.	1996	Articular cartilage	Solid	E 25 MPa, γ 0.4	[64]
Maurel et al.	1997	Gap between facet bones	Gap	–	[63]
de Jager et al.	1997	Gap between facet bone	Rigid, frictionless contact interaction	$Fc = b_f\ddot{u} + 2E + 9u^2$ for $0 \leqslant u < 3E - 4$ (m) $Fc = b_f\ddot{u} + 180 + 1.2E6(u - 3E - 4)$ for $u > 3E - 4$ (M) Fc– contact force b_f – damping coefficient (300 N s/m) u – penetration depth of facet bone $\ddot{u}$ – penetration speed	[31]
Yang et al.	1998	Gap between facet bone	Sliding contact interface	–	[67]
Goel et al.	1998	Gap between facet bones	Gap	Initial gap of 0.5 mm	[88]
Kumaresan et al.	1997–2000	Articular cartilage Synovial fluid Synovial membrane	Articular cartilage solid Synovial fluid – incompressible fluid Synovial membrane – membrane	Cartilage: E 10.4 MPa, γ 0.4 Synovial fluid: ρ 1000 kg/m^3 Synovial membrane: E 10–12 MPa, γ 0.4	[28,29,130,131,133]

[a] E: modulus of elasticity; γ: Poisson's ratio; k: stiffness; ρ: density.

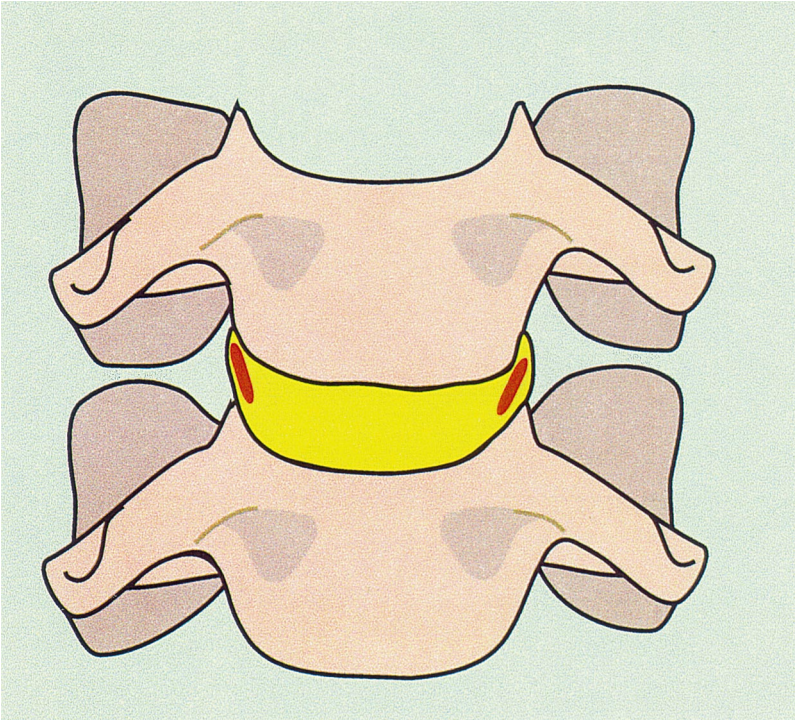

Fig. 8. Schematic of the bilateral uncovertebral (Luschka's) clefts.

ilar pattern was observed, the magnitudes of changes were higher (Fig. 11(b)). Facetectomy increased the angular motion and inferior disc stress; however, the adjacent superior disc stress was less significantly affected. Since facet resection beyond 50% produced accentuated angulations, the authors suggested that it may be necessary to stabilize the column with instrumentation during surgery. These increased internal stress changes in the disc may be more clinically pertinent than the external angulation change since increased stress (load) may enhance the degenerative process in the intervertebral components. These studies clearly highlight the importance of one soft tissue compromise on the external and internal responses of the spine and the remaining soft tissues.

6.2. Role of posterior ligamentous complex

In order to determine the contribution of this region under axial loading, the above intact (normal) model was modified [89]. All ligaments and zygapophysial joint structures dorsal to the posterior longitudinal ligament were inactivated. This was termed as the disc joint model while the former was termed as the intervertebral joint model. The overall external compressive stiffness was higher for the intervertebral joint model than the disc joint model. In contrast, the internal response indicated stress rises up to four times under compression in the disc joint model. This implies a higher role of the vertebral body due to the inability or loss of integrity of the posterior ligament complex. Since stress induction is responsible for osseous alterations, these added internal body stresses may lead to spondylotic changes in the anterior spinal column. Therefore, it was concluded that a compromise in the integrity of the posterior complex is critical to the load-carrying capacity of the cervical spine.

6.3. Role of interspinous ligament and ligamentum flavum resections: laminectomy

This detailed, complex finite element model was also used by our group to study the effects of transection of the ligamentum flavum and interspinous ligament, a procedure commonly used during laminectomy operations. The intact model response under flexion, extension, lateral bending, and axial torsion was compared with the laminectomized model response [30]. This included the external moment-rotation, and internal stresses in the superior and inferior discs; C4, C5, and C6 vertebral bodies; and C4 inferior, C5 superior, C5 inferior, and C6 superior endplates. Laminectomy altered the external angular motion and internal inferior disc stress under all loading modalities, with marked increases in flexion. Laminectomy with graded bilateral facet resections further enhanced these parameters. These increases emphasized the transfer of internal load sharing from the posterior to the anterior spine, thus demonstrating the destabilizing effects of laminectomy. The study supported the theory that cervical laminec-

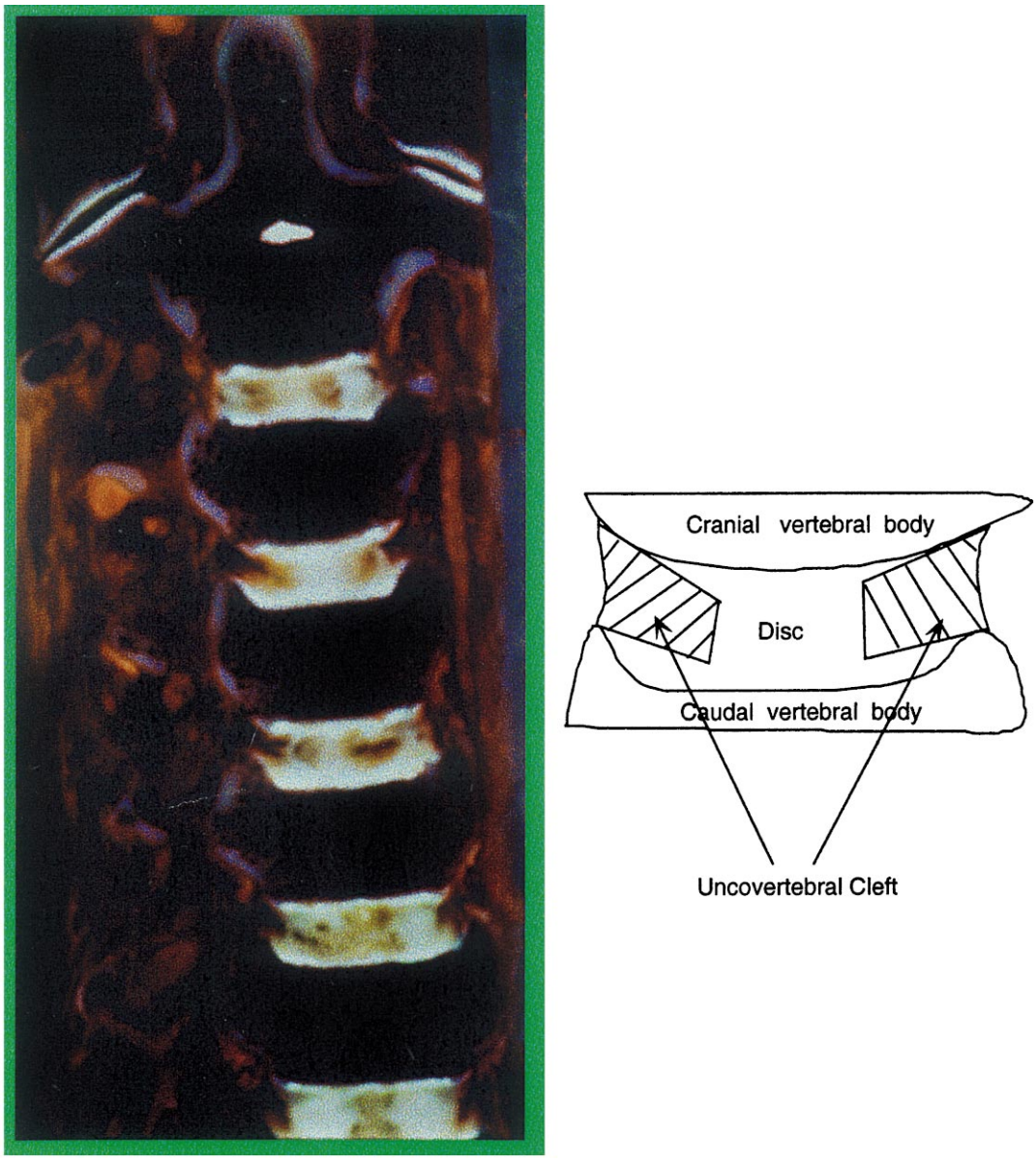

Fig. 9. (a) Coronal section of the human cervical spine. Left: frozen anatomic section of the human cervical spine showing the uncovertebral clefts at every level. Right: illustration of zygapophysial joint in magnified view. (b) Schematic of the idealized uncovertebral joints.

tomy accentuates degenerative changes in intervertebral disc tissues [124,125].

6.4. Role of anterior ligament transection and discectomy: fusion

The effects of two anterior fusion (surgical) procedures, secondary to anterior longitudinal ligament and disc removal, on the internal and external responses were evaluated by our group using the above C4–C5–C6 finite element model [126,127]. The internal responses included the disc and vertebral body stresses. Bailey–Badgley and Smith–Robinson procedures were simulated (Fig. 12) following anterior longitudinal and disc removal. Various fusion materials (titanium core, titanium cage, tricortical iliac graft, tantalum core, and tantalum cage) were used to evaluate the efficacy. In both procedures, the highest response was noted in the case of titanium core material followed by titanium cage, iliac crest, tantalum core, and tantalum cage. The Smith–Robinson procedure produced the highest increase in the external response under flexion, extension, lateral bending, and axial torsion. However, the Bailey–Badgley procedure resulted in higher increases in the disc and vertebral body stresses than the other technique (Fig. 13). These changes introduce different load-sharing patterns in the disc and other structures emphasizing the role of anterior longitudinal ligament rupture and discectomy on intervertebral biomechanics.

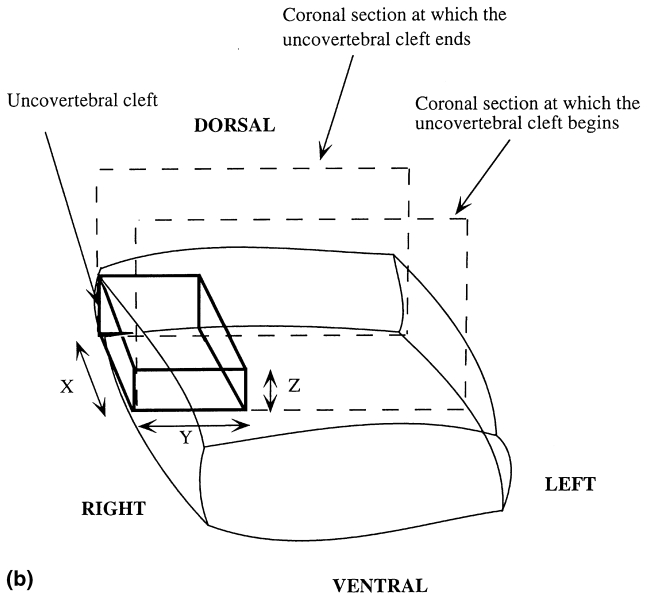

Fig. 9. (Continued).

6.5. Total disc load sharing

Another group developed a more simplified, one-level C5–C6 functional unit model (4219 nodes) which was based on 1.5-mm CT scans of a 68-year-old human cadaver [88]. The non-linear model was exercised at an axial compressive force of 74 N individually and in combination with pure moments of 1.8 N m in flexion, extension, lateral bending, or axial rotation. The interspinous and capsular ligaments sustained the most strains in flexion (29%) and axial rotation (15%), respectively. Maximum intradiscal pressure was the highest under combined compression and flexion (0.24 MPa). Load shared by the disc ranged from 14% in compression plus extension, 68% in right lateral bending, 75% in left axial rotation, 88% in compression, and 113% in compression plus flexion.

6.6. Role of uncovertebral joints

To understand the role of uncovertebral joints, the above model was modified [62]. The uncovertebral joints were simulated by using the properties of the anulus fibers of the disc. As an extension, surgical removal of uncinate processes was simulated with and without disturbing the integrity of uncovertebral joints. Results indicated that facet and uncovertebral joints contribute significantly to the coupled motions of the spine. While the uncinates decreased the primary and coupled motions (particularly in axial rotation and lateral bending), uncovertebral joints increased the kinematics.

Table 12
Uncovertebral cleft dimensions (mm) (Mean (SD)) [2][a]

Spinal level	Right side				Left side				Mean values		
	X	*Y*	*Z*		*X*	*Y*	*Z*		*X*	*Y*	*Z*
C2–C3	5	4.8 (1.4)	2.4 (0.4)		4	4.2 (1.4)	2.4 (0.6)		4.5 (0.7)	4.5 (1.4)	2.4 (0.5)
C3–C4	9	3.7 (2.1)	2.5 (1.1)		8	3.2 (1.0)	2.6 (0.9)		8.5 (0.7)	3.4 (1.7)	2.5 (1.0)
C4–C5	8	4.5 (2.0)	2.7 (0.9)		8	4.3 (2.8)	2.5 (1.0)		8 (0.0)	4.4 (2.4)	2.6 (0.9)
C5–C6	9	3.2 (1.9)	2.9 (0.8)		8	4.1 (0.9)	3.1 (0.5)		8.5 (0.7)	3.6 (1.9)	3.0 (0.6)
C6–C7	6	3.1 (0.7)	3.4 (0.5)		6	3.6 (1.7)	3.7 (0.5)		6.0 (0.0)	3.4 (1.3)	3.3 (0.5)
C7–T1	4	3.5 (1.6)	2.2 (0.3)		4	3.6 (1.7)	2.4 (0.5)		4.0 (0.0)	3.5 (1.6)	2.3 (0.4)

[a] *X*: dorsal-to-ventral length; *Y*: medial-to-lateral depth; *Z*: caudal-to-cranial height.

Table 13
Inclusion of uncovertebral cleft in mathematical models[a]

Author	Year	Uncovertebral joint components	Element idealization	Material properties	Reference
Goel et al.	1998	Gap between uncinates	Gap	–	[88]
Kumaresan et al.	1997–2000	Synovial fluid	Synovial fluid – Incompressible fluid	Fluid: ρ 1000 kg/m^3	[28,29,130,131,133]
		Synovial membrane	Synovial membrane – membrane	Membrane: E 10–12 MPa, γ 0.4	

[a] E: modulus of elasticity; ρ: density; γ: Poisson's ratio.

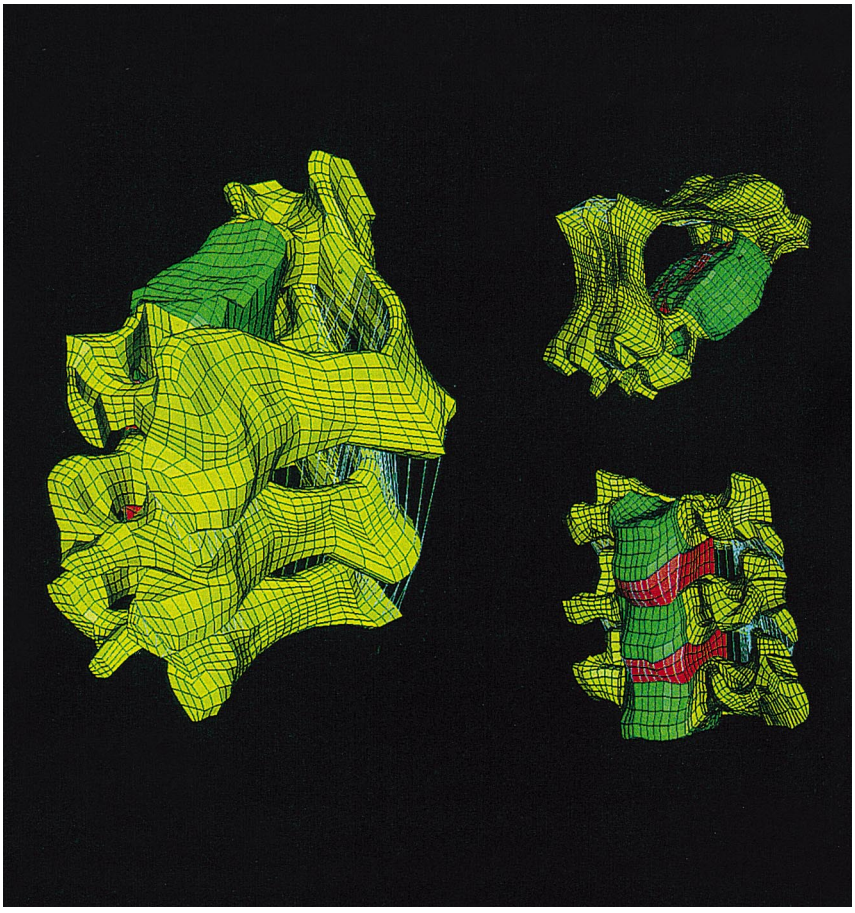

Fig. 10. Linear finite element model of the C4–C5–C6 cervical spine [70].

6.7. Regional load-sharing in the disc and uncovertebral joints

While the above studies individually examined the role of the entire disc or entire uncovertebral joints, studies conducted by our group hypothesized that differences in regional load sharing (ventral, middle, dorsal) contribute to the development of age-related spinal disorders such as osteophyte formations and disc herniations [28]. A previously developed three-dimensional geometrically and materially non-linear C4–C5–C6 finite element model was exercised under physiologic modes of combined loading, i.e., pure compression and varying degrees of compression–flexion and compression–extension (Fig. 14). Results indicated that the ventral region of the disc experienced higher axial forces under all loading modes. However, the dorsal region of the disc–uncovertebral joint anatomy experienced higher shear forces. The intra-discal pressure was the highest under the most severe compression–flexion loading. Data were compared with human volunteers and other experimental outcomes [128,129]. These accentuated internal, region-specific forces (axial in the ventral and shear in the dorsal) in the disc–uncoverte-

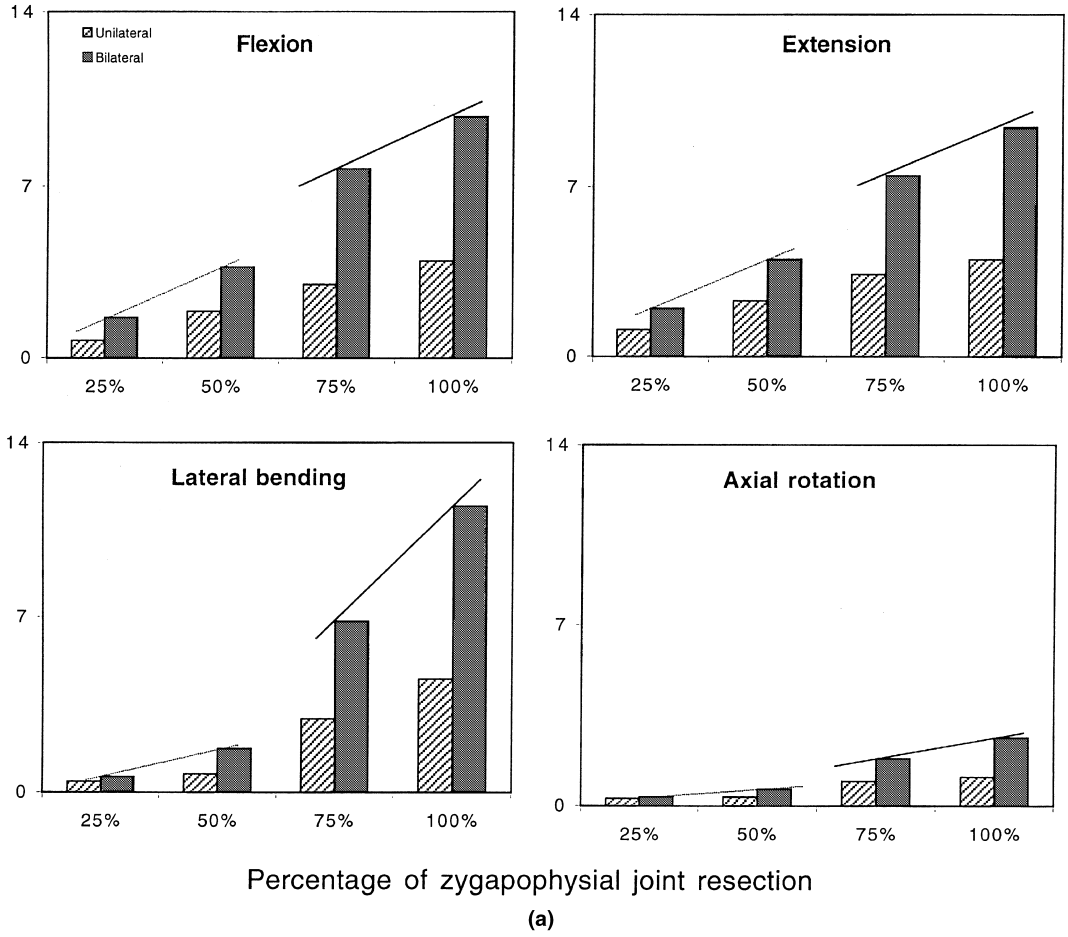

Fig. 11. (a) Percentage change of external (rotation) response from the intact spine due to graded facetectomies [107]. (b) Percentage change of internal disc (stress) response from the intact spine due to graded facetectomies [107].

bral joints formed a basis to explain the appearance of osteophytes spanning the anterior body–disc medium and disc herniations [28].

6.8. Role of soft tissue degeneration

Cervical spine disorders such as spondylotic radiculopathy and myelopathy are often related to osteophytes. To further explain this mechanism, the effects of varying degrees of cervical disc degeneration were investigated by our group on the internal stresses in the vertebral bodies using the non-linear model [130]. Four models were created: (a) intact (normal); (b) model with nucleus dehydration; (c) model with nucleus dehydration and anulus disintegration; and (d) model with nucleus dehydration and anulus disintegration and reduced disc height. The last three models represented slight, moderate, and severe cases of degeneration at one spinal level. The external overall and segmental stiffness increased with increasing levels of disc degeneration. However, the increase in stiffness was higher at the degenerated level (57% for the severe case) than the adjacent level (7%). The load shared by the disc and zygapophysial joints, and pressures in the nucleus, facet and uncovertebral joints showed minimal variations at the intact level. However, at the degenerated level, load transmitted through the zygapophysial joint and facet pressures decreased while the load shared by the disc joint increased. Disc bulge, anulus stress, and fiber strain of the degenerated disc decreased with increasing severity of degeneration. However, the responses of the bony cortex (stress and strain energy density) increased considerably with increasing degeneration. Increase in strain energy density/stress may accentuate bony changes and lead to bony outgrowth resulting in osteophytes. Changes in facet load distribution due to disc and/or facet degeneration may also explain the structural compromise in the integrity of the zygapophysial joint leading to disorders such as facet arthritis in the cervical spine.

6.9. Models of developmental pediatric cervical spine

Our group advanced finite element modeling efforts to study the flexibility responses of age specific one-, three-, and six-year-old pediatric models (Fig. 15) [29,90,121,131–133]. Since skeletal developments occur

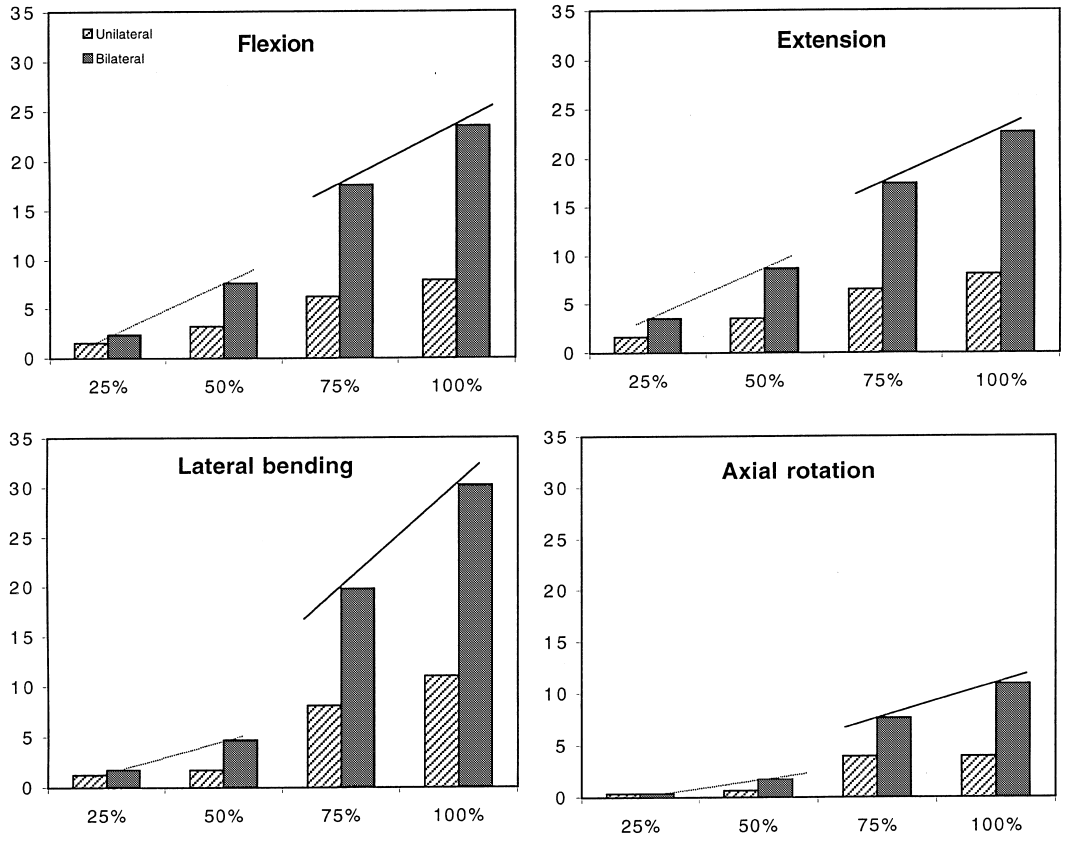

Fig. 11. (Continued).

during the growing years, in a sense, a majority of the load-bearing components are soft tissues. Cartilages and growth plates essentially surround vertebrae. For these three age groups, flexibility responses were obtained and compared with the above-determined adult responses under pure compression, pure tension, pure flexion moment and pure extension moment, and varying degrees of combined compression–flexion and compression–extension. Results indicated that the inclusion of developmental soft tissue-related anatomical changes have a predominant effect on the biomechanical responses. It was concluded that it is imperative to appropriately simulate all the necessary anatomically related components (soft tissue) in order to realistically predict age-specific pediatric responses.

7. Summary

Responses and contributions of the soft tissue structures of the human neck from a mathematical modeling perspective are presented. Spinal ligaments, intervertebral discs, zygapophysial joints, and uncovertebral joints of the cervical spine are included. Finite element modeling approaches have been emphasized. A brief discussion is provided on the developmental biomechanics of the pediatric spine with a focus on soft tissues. Although not all inclusive, representative data relevant to the development and execution of the model are discussed. A brief description of the functional mechanical role of all soft tissue components is given. Geometrical characteristics such as length and cross-sectional areas, and material properties such as force–displacement and stress–strain responses, are described. A summary of the finite element modeling approaches for each soft tissue structure is presented. The final discussion emphasizes the normal and abnormal (e.g., due to degenerative joint disease, iatrogenic alteration, trauma) behaviors of the cervical spine with a focus on all these soft tissue responses. Although not specifically discussed in this paper, it is necessary that the finite element model or, as a matter of fact, any mathematical model be validated with controlled experimental data to provide realistic estimations of the external and internal responses of the soft and hard tissue structures of the cervical spine. Only when the model is based on accurate geometry, material property, boundary and loading conditions, and experimentally validated, will it be use-

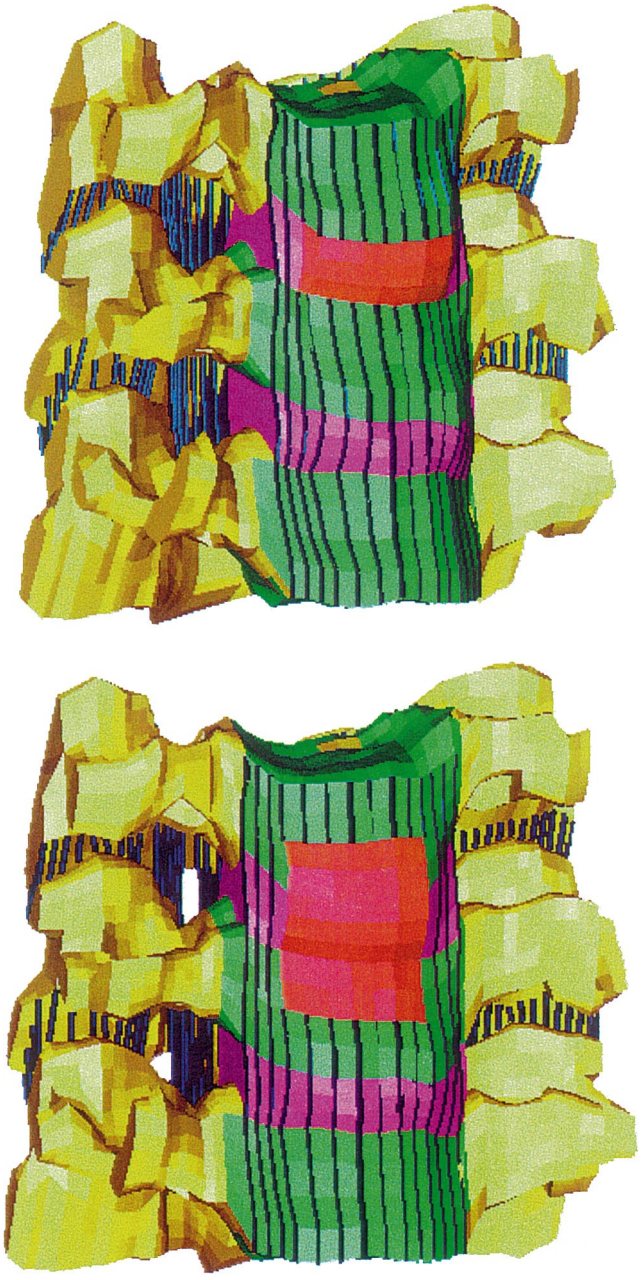

Fig. 12. Finite element models of Smith–Robinson (top) and Bailey–Badgley surgical techniques [127].

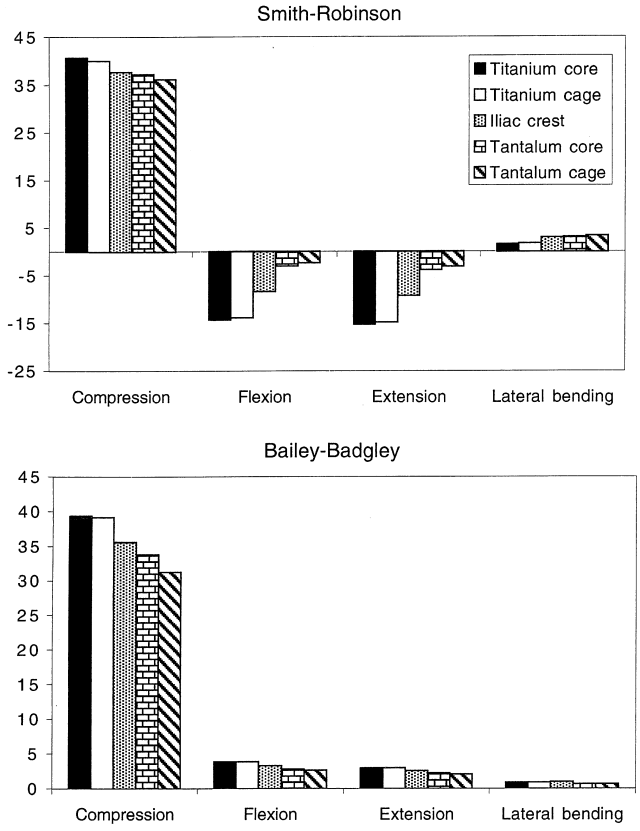

Fig. 13. Comparison of the changes in internal disc stress (percentage change from the intact spine) between Smith–Robinson (top) and Bailey–Badgley (bottom) techniques compared to intact (normal) condition [127].

ful to delineate the clinical biomechanics of the spine under various conditions. Since soft tissues control the complex response, an accurate simulation of their anatomic, functional, and biomechanical characteristics is necessary to investigate in detail the behavior of the normal and abnormal cervical spine structures.

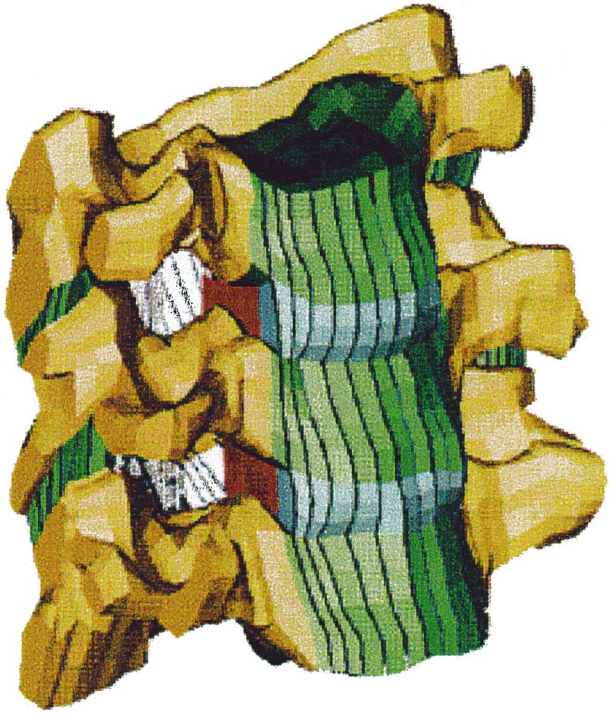

Fig. 14. Detailed non-linear finite element model of the C4–C5–C6 spine used to explain the formation of osteophytes and disc herniations under physiologic modes of loading [28].

Acknowledgements

This research was supported in part by PHS CDC R49CCR 515433, NHTSA DTNH22-93-Y-17028, and VA Medical Research.

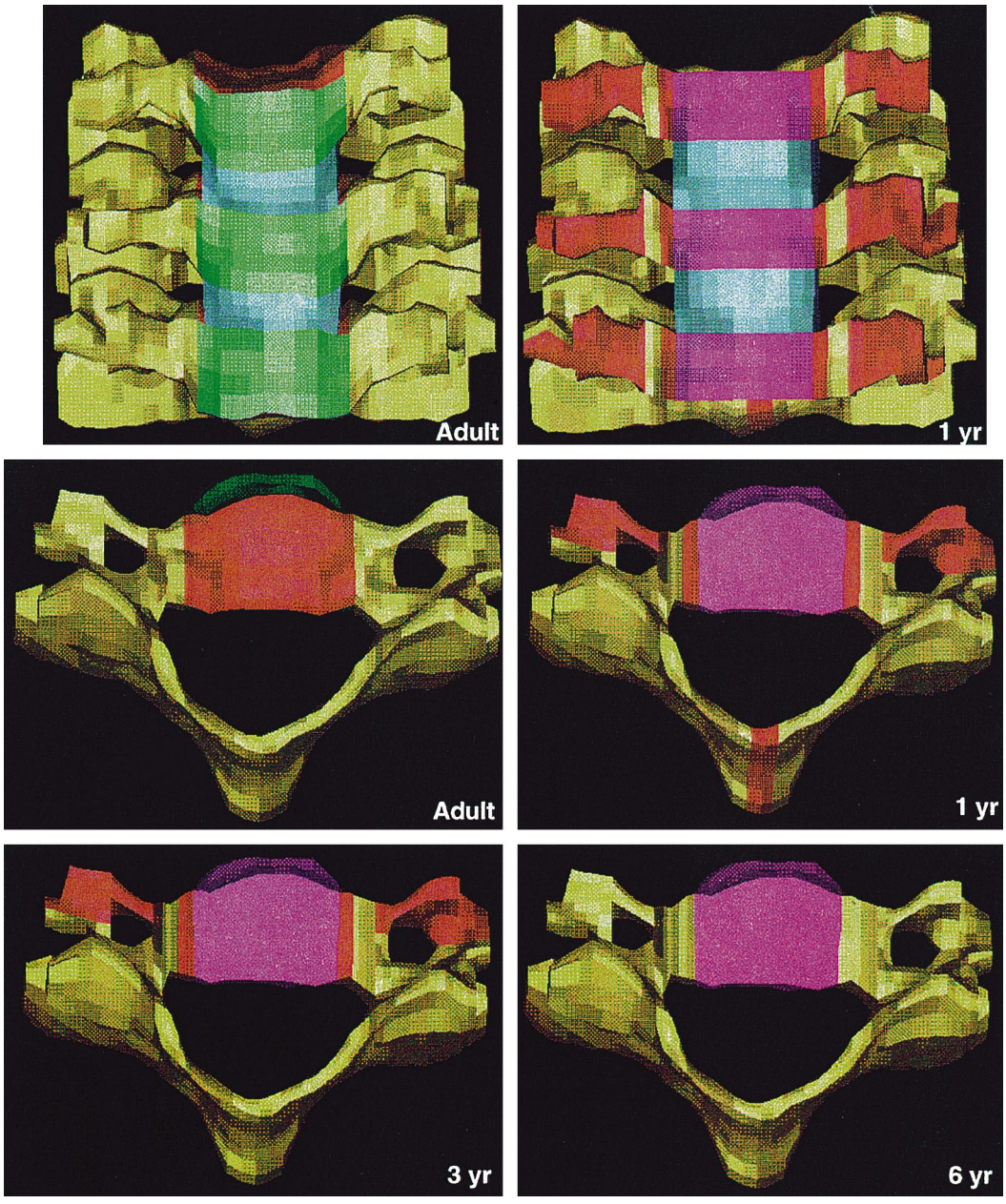

Fig. 15. Finite element models of the age-specific cervical spine emphasizing developmental anatomy differences. Upper left: frontal view, adult model; upper right: frontal view, one-year-old; middle left: superior view, C5 adult; middle right: superior view, C5 one-year-old; lower left: superior view, C5 three-year-old; lower right: superior view, C5 six-year-old. The images are not to scale [29].

Appendix A. Typical force–displacement/stress–strain behavior

The response is non-linear; often this is referred to as the sigmoidal curve. In order to better understand this behavior, the derivative of force with respect to displacement, i.e., stiffness–deflection response, is computed [3–6,46]. As can be identified from Fig. 2, in the initial stages of loading (region OA), the structure responds with a gradual increase in load with increasing deflection, i.e., a gradual increase of stiffness (OA^1). This is termed the ambient phase or toe region. The ligament fibers from a mechanical perspective align during this initial phase (OA) and, therefore, the load and hence the stiffness increases gradually. This change in ligament fiber alignment is manifested by an increase in stiffness with additional loading. During this stage, the response becomes linear (region AB), reaching a level of almost constant stiffness (A^1B^1). This region represents the most resistive nature of the structure, and is termed as the physiologic loading phase. It should be noted that the initial toe region is also included in this definition. With additional increase in external tensile load, the response becomes more non-linear (region BC) with a

gradual drop of stiffness (B^1C^1). The point at which this drop begins is the end of physiologic loading phase, and the subsequent region wherein the specimen has begun to exhibit gradual decrease in stiffness (B^1C^1) is termed as the traumatic loading phase. At the end of this traumatic phase, the specimen has totally lost its structural integrity and fails (point C) with a zero stiffness (point C^1). The "falling off" portion of the curve beyond this region is termed the post-traumatic phase (similar to post-buckling behavior). From a mechanistic basis, the structure is capable of fully and effectively absorbing/transmitting the load in the physiologic range without any compromise in its integrity, and microlevel failures in the form of fiber tears begin to occur when it is loaded beyond this physiologic range [3–5,46]. These physiologic, traumatic, and post-traumatic phases have been reclassified into neutral, elastic, and plastic zones, respectively [7].

References

[1] Wolfla CE. Adult and child and neck anatomy. In: Yoganandan N, Pintar FA, Larson SJ, Sances A, editors. Frontiers in head and neck trauma: clinical and biomechanical. The Netherlands: IOS Press, 1998. p. 18–33.

[2] Kumaresan S, Yoganandan N, Pintar FA. Methodology to quantify the uncovertebral joint in the human cervical spine. J Musculoskeletal Res 1997;1:1–9.

[3] Yoganandan N, Pintar FA, Myklebust JB, Maiman DJ, Sances AJ, Larson SJ. Initiation of injury in cervical spine segments. In: Proceedings of 13th Annual Meeting of Cervical Spine Research Society. Boston, MA, 1985.

[4] Yoganandan N, Ray G, Sances Jr A, Pintar FA, Myklebust J, Maiman DJ, Myers T. Assessment of traumatic failure load and microfailure load in an intervertebral disc segment. ASME Adv Bioeng 1985:130–1.

[5] Yoganandan N, Ray G, Pintar FA, Myklebust JB, Sances A. Stiffness and strain energy criteria to evaluate the threshold of injury to an intervertebral joint. J Biomech 1989;22:135–42.

[6] Yoganandan N, Halliday A, Dickman C, Benzel E. Practical anatomy and fundamental biomechanics. In: Benzel E, editor. Spine surgery: techniques, complication avoidance and management. New York, NY: Churchill Livingstone, 1999. p. 93–118.

[7] White AA, Panjabi MM. Clinical biomechanics of the spine, second ed.. Philadelphia, PA: J.B. Lippincott; 1990.

[8] Maiman DJ, Yoganandan N. Biomechanics of cervical spine trauma. In: Black P, editor. Clinical neurosurgery. Baltimore, MD: Williams & Wilkins; 1991. p. 543–70.

[9] Hukins DWL. Disc structure and function. In: Ghosh P, editor. Biology of the intervertebral disc. Boca Raton, FL: CRC Press, 1988. p. 1–33.

[10] Coventry MB, Ghormley RK, Kernohan JW. The intervertebral disc: its microscopic anatomy and pathology. Part II: Changes in the intervertebral disc concomitant with age. J Bone Jt Surg 1945;27:233–47.

[11] Cusick JF, Yoganandan N, Pintar FA, Myklebust JB, Hussain H. Biomechanics of cervical spine facetectomy and fixation techniques. Spine 1988;13:808–12.

[12] Wen N, Lavaste F, Santin J, Lassau J. Three-dimensional biomechanical properties of the human cervical spine in vitro. Eur Spine J 1993;2:2–15.

[13] Moroney SP, Schultz AB, Miller JA, Andersson GB. Load-displacement properties of lower cervical spine motion segments. J Biomech 1988;21:769–79.

[14] Shea M, Edwards WT, White III AA, Hayes WC. Variations of stiffness and strength along the human cervical spine. J Biomech 1991;24:95–107.

[15] Yoganandan N, Pintar FA, Maiman DJ, Cusick JF, Sances Jr A, Walsh PR. Human head–neck biomechanics under axial tension. Med Eng Phys 1996;18:289–94.

[16] Cusick JF, Pintar FA, Yoganandan N, Reinartz JM. Biomechanical alterations induced by multilevel cervical laminectomy. Spine 1995;20:2393–9.

[17] Pintar FA, Yoganandan N, Myers T, Elhagediab A, Sances Jr A. Biomechanical properties of human lumbar spine ligaments. J Biomech 1992;25:1351–6.

[18] Yoganandan N, Pintar FA, Cusick JF, Kleinberger M. Head–neck biomechanics in simulated rear impact. In: Proceedings of the 42nd Association for the Advancement of Automotive Medicine. Charlottesville, VA, 1998. p. 209–31.

[19] Yoganandan N, Sances Jr A, Pintar FA. Biomechanical evaluation of the axial compressive responses of the human cadaveric and manikin necks. J Biomech Eng 1989;111:250–5.

[20] Yoganandan N, Pintar FA, Cusick JF. Biomechanics of compression–extension injuries to the cervical spine. In: Proceedings of the 41st Association for the Advancement of Automotive Medicine. Orlando, FL; 1997. p. 331–44.

[21] Yoganandan N, Sances Jr A, Maiman DJ, Myklebust JB, Pech P, Larson SJ. Experimental spinal injuries with vertical impact. Spine 1986;11:855–60.

[22] Nusholtz GS, Huelke DE, Luz P, Alem NM, Montavo F. Cervical spine injury mechanisms. In: Proceedings of 27th Stapp Car Crash Conference. San Diego, CA, 1983. p. 179–98.

[23] Culver R, Bender M, Melvin J. Mechanisms, tolerances, and responses obtained under dynamic superior–inferior head impact. Ann Arbor, MI: Univ Michigan, 1978. p. 103.

[24] Alem NM, Nusholtz GS, Melvin JW. Head and neck response to axial impacts. In: Proceedings of 28th Stapp Car Crash Conference. Warrendale, PA, 1984. p. 275–88.

[25] Ewing C, Thomas D, Sances Jr A, Larson SJ, editors. Impact injury of the head and spine. Springfield, IL: Thomas, 1983.

[26] Yoganandan N, Sances Jr A, Pintar FA, Maiman DJ, Reinartz J, Cusick JF, Larson SJ. Injury biomechanics of the human cervical column. Spine 1990;15:1031–9.

[27] Maiman DJ, Sances Jr A, Myklebust JB, Larson SJ, Houterman C, Chilbert M, El-Ghatit AZ. Compression injuries of the cervical spine: A biomechanical analysis. Neurosurgery 1983;13:254–60.

[28] Kumaresan S, Yoganandan N, Pintar FA, Maiman DJ. Finite element modeling of the lower cervical spine: role of intervertebral disc under axial and eccentric loads. Med Eng Phys 1999;21:689–700.

[29] Kumaresan S, Yoganandan N, Pintar FA, Maiman DJ, Kuppa S. Biomechanical study of pediatric human cervical spine: a finite element approach. J Biomech Eng 2000;122:60–71.

[30] Kumaresan S, Yoganandan N, Pintar FA, Voo L, Cusick JF, Larson SJ. Finite element modeling of cervical laminectomy with graded facetectomy. J Spinal Disord 1997;10:40–7.

[31] Maurel N, Lavaste F, Skalli W. A three-dimensional parameterized finite element model of the lower cervical spine. Study of the influence of the posterior articular facets. J Biomech 1997;30:921–31.

[32] Yoganandan N, Kumaresan S, Voo L, Pintar FA. Finite element applications in human cervical spine modeling. Spine 1996;21:1824–34.

[33] Yoganandan N, Myklebust JB, Ray G, Sances Jr A. Mathematical and finite element analysis of spinal injuries. CRC Rev Biomed Eng 1987;15:29–93.

[34] Kumaresan S, Yoganandan N, Pintar FA. Finite element analysis of the cervical spine: a material property sensitivity study. Clin Biomech 1999;14:41–53.
[35] Myklebust JB, Pintar FA, Yoganandan N, Cusick JF, Maiman DJ, Myers T, Sances Jr A. Tensile strength of spinal ligaments. Spine 1988;13:526–31.
[36] Yoganandan N, Pintar FA, Butler J, Reinartz J, Sances Jr A, Larson SJ. Dynamic response of human cervical spine ligaments. Spine 1989;14:1102–10.
[37] Yoganandan N, Kumaresan S, Pintar FA. Geometrical and mechanical properties of human cervical spine ligaments. J Biomech Eng 2000; in press.
[38] Menezes A, Sonntag V. Principles of spinal surgery. New York: McGraw-Hill, 1996.
[39] Panjabi MM, Oxland TR, Parks EH. Quantitative anatomy of cervical ligaments. Part II. Middle and lower cervical spine. J Spinal Disord 1991;4:276–85.
[40] Przybylski GJ, Patel PR, Carlin GJ, Woo S. Quantitative anthropometry of the subatlantal cervical longitudinal ligaments. Spine 1998;23:893–8.
[41] Mercer S, Bogduk N. The ligaments and anulus fibrosus of human adult cervical intervertebral discs. Spine 1999;24:619–28.
[42] Rauschning W. Surface cryoplaning – a technique for clinical anatomical correlations. Ups J Med Sci 1986;91:251–5.
[43] Pech P, Bergstrom K, Rauschning W, Haughton WM. Attenuation values, volume changes and artifacts in tissue due to freezing. Acta Radiol 1987;28:779–82.
[44] Yoganandan N, Pintar FA, Kumaresan S, Elhagediab A. Biomechanical assessment of human cervical spine ligaments. In: Proceedings of the 42nd Stapp Car Crash Conference, 1998. p. 223–36.
[45] Chazal J, Tanguy A, Bourges M. Biomechanical properties of spinal ligaments and a histological study of the supraspinal ligament in traction. J Biomech 1985;18:167–76.
[46] Yoganandan N, Maiman DJ, Pintar FA, Ray G, Myklebust JB, Sances Jr A, Larson SJ. Microtrauma in the lumbar spine: a cause of low back pain. Neurosurgery 1988;23:162–8.
[47] Pintar FA, Yoganandan N, Voo LM. Effect of age and loading rate on human cervical spine injury threshold. Spine 1998;23:1957–62.
[48] Backaitis SH, editor. Biomechanics of impact injury and injury tolerances of the head-neck complex. Warrendale, PA: Society of Automotive Engineers, PT43, 1993.
[49] Cesari D, Ramet M. Pelvic tolerance and protection criteria in side impact. In: Proceedings of the 26th Stapp Car Crash Conference. Warrendale, PA, 1982. p. 145–54.
[50] McElhaney JH, Roberts VL, Hilyard JF, Handbook of human tolerance. Tokyo, Japan: Japan Automobile Research Institute, 1976.
[51] Huelke DF, Nusholtz GS. Cervical spine biomechanics: a review of the literature. J Orthop Res 1986;4:232–45.
[52] Errico TJ, Bauer RD, Waugh T. Spinal trauma. Philadelphia: J.B. Lippincott; 1991. p. 656.
[53] Clark CR, Ducker TB, Dvorak J, Garfin SR, Herkowitz HN, Levine AM, Pizzutillo PD, Ulrich CG, Zeidman SM. The cervical spine. 3rd ed. Philadelphia, PA: Lippincott-Raven, 1998. p. 1003.
[54] Herkowitz HN, Garfin SR, Balderston RA, Eismont FJ, Bell GR, Wiesel SW. The spine. 3rd ed. Saunders, 1992.
[55] Yoganandan N, Pintar FA, Cusick JF, Reinartz J, Sances AJ, Maiman DJ. Cervical spine injury mechanism under vertical impact. ASME-BED 1994;28:339–40.
[56] Yoganandan N, Haffner M, Maiman DJ, Nichols H, Pintar FA, Jentzen J, Weinshel S, Larson SJ, Sances Jr A. Epidemiology and injury biomechanics of motor vehicle related trauma to the human spine. SAE Trans 1990;98:1790–1807.
[57] Yoganandan N, Pintar FA, Sances Jr A, Maiman DJ. Strength and motion analysis of the human head–neck complex. J Spinal Disord 1991;4:73–85.
[58] Yoganandan N, Maiman DJ, Pintar FA. Biomechanics of the cervical spine. In: Menezes A, Sonntag V, editors. Principles of spinal surgery. New York: McGraw-Hill, 1996. p. 69–83.
[59] Chang H, Gilbertson LG, Goel VK, Winterbottom JM, Clark CR, Patwardhan A. Dynamic response of the occipito–atlanto–axial (C0–C1–C2) complex in right axial rotation. J Orthopaedic Res 1992;10:446–53.
[60] Yoganandan N, Pintar FA, Maltese MM. Biomechanics of abdominal injuries. Crit Rev Bioeng 2000; In press.
[61] Yoganandan N, Pintar FA, Sances Jr A, Maiman DJ, Myklebust J, Harris G, Ray G. Biomechanical investigations of the human thoracolumbar spine. SAE Trans 1989;97:676–81.
[62] Clausen JD, Goel VK, Traynelis VC, Scifert J. Uncinate processes and Luschka joints influence the biomechanics of the cervical spine: quantification using a finite element model of the C5–C6 segment. J Orthop Res 1997;15:342–7.
[63] de Jager M, Sauren A, Thunnissen J, Wismans J. A three-dimensional head-neck model: validation for frontal and lateral impacts. In: Proceedings of the 38th Stapp Car Crash Conference. Ft. Lauderdale, FL; 1994. p. 93–109.
[64] Nitsche S, Krabbel G, Appel H, Haug E. Validation of a finite-element-model of the human neck. In: Proceedings of the International Conference on the Biomechanics of Impact. Dublin, Ireland, 1996. p. 107–8.
[65] Kleinberger M. Application of finite element techniques to the study of cervical spine mechanics. In: Proceedings of the 37th Stapp Car Crash Conference. San Antonio, TX; 1993. p. 261–72.
[66] Dauvilliers F, Bendjellal F, Weiss M, Lavaste F, Tarriere C. Development of a finite element model of the neck. In: Proceedings of the 38th Stapp Car Crash Conference. Ft. Lauderdale, FL, 1994. p. 77–91.
[67] Yang K, Zhu F, Luan F, Zhao L, Begeman P. Development of a finite element model of the human neck. In: Proceedings of the 42nd Stapp Car Crash Conference. Ft. Lauderdale, FL, 1998. p. 195–205.
[68] Saito T, Yamamuro T, Shikata J, Oka M, Tsutsumi S. Analysis and prevention of spinal column deformity following cervical laminectomy: pathogenetic analysis of postlaminectomy deformities. Spine 1991;16:494–502.
[69] Yoganandan N, Voo L, Pintar FA, Kumaresan S, Cusick JF, Sances Jr A. Finite element analysis of the cervical spine. In: Proceedings of Injury Prevention Through Biomechanics. Detroit, MI, 1995. p. 149–55.
[70] Yoganandan N, Kumaresan S, Voo L, Pintar FA, Larson SJ. Finite element modeling of the C4-C6 cervical spine unit. Med Eng Phy 1996;18:569–74.
[71] Yoganandan N, Kumaresan S, Voo L, Pintar FA. Finite element model of the human lower cervical spine. J Biomech Eng 1997;119:87–92.
[72] Nachemson A, Evans J. Some mechanical properties of the third lumbar inter-laminar ligament ligamentum flavum. J Biomech 1968;1:211–7.
[73] Tkaczuk H. Tensile properties of human lumbar longitudinal ligaments. Acta Orthop Scand 1968;115:1–91.
[74] Hukins D, Kirby M, Sikoryn T, Aspden R, Cox A. Comparison of structure, mechanical properties and functions of lumbar spinal ligaments. Spine 1990;15:787–95.
[75] Kumaresan S, Yoganandan N, Pintar FA. Finite element modeling of spinal ligaments. In: Proceedings of the ASME Adv Bioeng, 1999. p. 233–4.
[76] Pintar FA, Yoganandan N, Pesigan M, Reinartz JM, Sances Jr A, Cusick JF. Cervical vertebral strain measurements under axial and eccentric loading. J Biomech Eng 1995;117:474–8.

[77] Matsunaga S, Kabayama S, Yamamoto T, Yone K, Sakou T, Nakanishi K. Strain on intervertebral discs after anterior cervical decompression and fusion. Spine 1999;24:670–5.
[78] Penning L. Differences in anatomy, motion, development and aging of the upper and lower cervical disk segments. Clin Biomech 1988;3:37–47.
[79] Pooni JS, Hukins DW, Harris PF, Hilton RC, Davies KE. Comparison of the structure of human intervertebral discs in the cervical, thoracic and lumbar regions of the spine. Surg Radiol Anat 1986;8:175–82.
[80] Gilad I, Nissan M. A study of vertebra and disc geometric relations of the human cervical and lumbar spine. Spine 1986;11:154–7.
[81] Panjabi MM, Duranceau J, Goel VK. Cervical human vertebrae quantitative three-dimensional anatomy of the middle and lower regions. Spine 1991;16:861–9.
[82] Nissan M, Gilad I. The cervical and lumbar vertebrae: an anthropometric model. Eng Med 1984;13:111–4.
[83] Yoganandan N, Pintar FA, Kumaresan S. Unpublished data.
[84] Zidel P, Ngai J, Raynor R, Hobbs G, Pugh J. Three-dimensional analysis of cervical spine motion segments by computer video-photogrammetry. In: Proceedings of the 31st Annual ORS. Las Vegas, NV, 1985. p. 330.
[85] Pintar FA, Myklebust JB, Yoganandan N, Sances Jr A. Biomechanical properties of the human intervertebral disc in tension. In: Proceedings of the ASME. New York, NY, 1986. p. 38–39.
[86] Wu HC, Yao RF. Mechanical behavior of the human anulus fibrosus. J Biomech 1976;9:1–7.
[87] Yamada H. In: Evans FG, editor. Strength of biological materials. Baltimore, MD: Williams & Wilkins, 1970. p. 297.
[88] Goel VK, Clausen JD. Prediction of load sharing among spinal components of a C5–C6 motion segment using the finite element approach. Spine 1998;23:684–91.
[89] Kumaresan S, Yoganandan N, Pintar FA. Posterior complex contribution to the axial compressive and distraction behavior of the cervical spine. J Musculoskeletal Res 1998;2:257–65.
[90] Kumaresan S, Yoganandan N, Pintar FA. Pediatric neck modeling using finite element analysis. Int J Crashworthiness 1998;2:367–77.
[91] Williams JL, Belytschko TB. A three-dimensional model of the human cervical spine for impact simulations. J Biomech Eng 1983;105:321–31.
[92] Nowitzke A, Westaway M, Bogduk N. Cervical zygapophysial joints: geometrical parameters and relationship to cervical kinematics. Clin Biomech 1994;9:342–7.
[93] Milne N. The role of zygapophysial joint orientation and uncinate processes in controlling motion in the cervical spine. J Anat 1991;178:189–201.
[94] Onan O, Heggeness M, Hipp J. A motion analysis of the cervical facet joint. Spine 1998;23:430–9.
[95] Tobias D, Ziv I, Maroudas A. Human facet cartilage: swelling and some physico-chemical characteristics as a function of age. Spine 1992;17:694–700.
[96] Bogduk N, Marsland A. The cervical zygapophysial joint as a source of neck pain. Spine 1988;13:610–7.
[97] Bogduk N. Pathoanatomical assessment of whiplash. In: Yoganandan N, Pintar F, Larson S, Sances A, editors. Frontiers in head and neck trauma: clinical and biomechanical. The Netherlands: IOS Press, 1998.
[98] Aprill C, Dwyer A, Bogduk N. Cervical zygapophysial joint pain patterns II: a clinical evaluation. Spine 1990;15:458–61.
[99] Bogduk N, Aprill C. The prevalence of cervical zygapophysial joint pain, a first approximation. Spine 1993;17:744–7.
[100] Lord S, Bogduk N, Barnsley L. Prevalence of third occipital headache following whiplash. Orthop Trans 1992.
[101] Yoganandan N, Pintar FA, Kleinberger M. Whiplash injury – biomechancial experimentation. Spine 1999;24:83–5.
[102] Cusick JF, Yoganandan N, Pintar FA, Gardon M. Cervical spine injuries from high velocity forces: a pathoanatomical and radiological study. J Spinal Disord 1996;9:1–7.
[103] Yoganandan N, Pintar FA, Cusick JF. Biomechanical analyses of whiplash injuries using experimental model. In: Proceedings of the World Congress Whiplash Associated Disorders. Vancouver, Canada, 1999. p. 325–43.
[104] Yoganandan N, Pintar FA. Mechanisms of headache and neck pain in whiplash. In: Yoganandan N, Pintar FA, editors. Frontiers in whiplash trauma: clinical & biomechanical. The Netherlands: IOS Press, 2000.
[105] Ahmed AM, Duncan NA, Burke DL. The effect of facet geometry on the axial torque-rotation response of lumbar motion segments. Spine 1988;15:391–401.
[106] Zdeblick TA, Abitbol JJ, Kunz DN, McCabe RP, Garfin S. Cervical stability after sequential capsule resection. Spine 1993;18:2005–8.
[107] Voo L, Kumaresan S, Yoganandan N, Pintar FA, Cusick JF. Finite element analysis of cervical facetectomy. Spine 1997;22:964–9.
[108] Raynor RB, Moskovich R, Zidel P, Pugh J. Alterations in primary and coupled neck motions after facetectomy. Neurosurgery 1987;21:681–7.
[109] Francis CC. Variations in the articular facets of the cervical vertebrae. Anat Rec 1955;122:589–602.
[110] Panjabi MM, Oxland T, Takata K, Goel VK, Duranceau J, Krag M. Articular facets of the human spine: quantitative three dimensional anatomy. Spine 1993;10:1298–310.
[111] Kumaresan S, Yoganandan N, Pintar FA. Finite element modeling approaches of human cervical spine facet joint capsule. J Biomech 1998;31:371–6.
[112] Tonetti J, Peoch M, Merloz P, Pasquier B, Chirossel J. Elastic reinforcement and thickness of the joint capsules of the lower cervical spine. Surgic Radiol Anat 1999;21:35–9.
[113] Mercer S, Bogduk N. Intra-articular inclusions of the cervical synovial joints. Brit J Rheum 1993;32:705–10.
[114] Kempson GE. Mechanical properties of articular cartilage. In: Adult articular cartilage. Kent, England: Pitman, 1979. p. 333–414.
[115] Sherk HH, Dunn EJ, Eismont FJ, Fielding JW, Long DM, Ono K, Penning L, Raynor R. The cervical spine, 2nd ed. Philadelphia, PA: Lippincott, 1989.
[116] Hall MC. Luschka's joint. Springfield, IL: Thomas, 1965. p. 141.
[117] Boreadis AG, Gershon-Cohen J. Luschka joints of the cervical spine. Radiology 1956;66:181–7.
[118] Compere EL, Tachdjian MO, Kernahan WT. The luschka joints: their anatomy, physiology and pathology. Orthopaedics 1959;1:159–68.
[119] Penning L. Functional anatomy of joints and discs. In: Sherk HH, Dunn EJ, Eismont FJ, editors. The cervical spine. Philadelphia, PA: Lippincott, 1989. p. 33–56.
[120] Penning L, Wilmink JT. Rotation of the cervical spine. A CT study in normal subjects. Spine 1987;12:732–8.
[121] Kumaresan S, Yoganandan N, Pintar FA, Reichert K. Dynamic analysis of pediatric cervical spine. In: Proceedings of the IEEE BMES/EMBS Joint Conference, 1999. p. 507.
[122] Zdeblick TA, Zou D, Warden KE, McCabe R, Kunz D, Vanderby R. Cervical stability after foraminotomy. J Bone Jt Surg 1992;74A:22–7.
[123] Raynor RB, Pugh J, Shapiro I. Cervical facetectomy and its effect on spine strength. J Neurosurg 1985;63:278–82.
[124] Ishida Y, Suzuki K, Ohmori K, Kikata Y, Hattori Y. Critical analysis of extensive cervical laminectomy. Neurosurgery 1989;24:215–22.
[125] Cahill D, Bellegarrigue R, Ducker T. Bilateral facet to spinous process fusion: a new technique for posterior spinal fusion after trauma. Neurosurgery 1983;13:1–4.

[126] Maiman DJ, Kumaresan S, Yoganandan N, Pintar FA. Effect of anterior cervical interbody fusion on adjacent segments. Biomed Mater Eng 1999;9:27–38.
[127] Kumaresan S, Yoganandan N, Pintar FA. Finite element analysis of anterior cervical spine interbody fusion. Biomed Mater Eng 1997;7:221–30.
[128] Hattori S, Oda H, Kawai S. Cervical intradiscal pressure in movements and traction of the cervical spine. Z Orthop 1981;119:568.
[129] Pospiech J, Stolke D, Wilke H, Claes L. Intradiscal pressure recordings in the cervical spine. Neurosurgery 1999;44:379–85.
[130] Kumaresan S, Yoganandan N, Pintar FA, Maiman DJ, Goel VK. Contribution of disc degeneration to osteophyte formation in cervical spine: biomechanical model. J Orthop Res 2000;Under Review.
[131] Kumaresan S, Yoganandan N, Pintar FA. Biomechanics of pediatric cervical spine: compression, flexion and extension responses. J Crash Prevention Injury Control 2000;2:87–101.
[132] Yoganandan N, Kumaresan S, Pintar FA. Pediatric cervical spine biomechanics using finite element models. In: Proceedings of the International Research Council on the Biomechanics of Impact. Goteborg, Sweden, 1998. p. 349–63.
[133] Kumaresan S, Yoganandan N, Pintar FA. Age-specific pediatric cervical spine biomechanical responses: Three-dimensional nonlinear finite element models. In: Proceedings of the 41st Stapp Car Crash Conference. Orlando, FL, 1997. p. 31–61.